Multi-stable and spatiotemporal staggered patterns in a predator-prey model with predator-taxis and delay

Weihua Jiang[1], Yue Xing—[1], and Xun Cao[1]

[1]Harbin Institute of Technology School of Mathematics

January 12, 2023

Abstract

The effects of predator-taxis and conversion time delay on formations of spatiotemporal patterns in a predator-prey model are explored. Firstly, the well-posedness, which implies global existence of classical solutions, is proved. Then, we establish critical conditions for the destabilization of coexistence equilibrium through Turing/Turing-Turing bifurcations via describing the first Turing bifurcation curve, and theoretically predict possible bi-stable/multi-stable spatially heterogeneous patterns. Next, we demonstrate that coexistence equilibrium can also be destabilized through Hopf, Hopf-Hopf, Turing-Hopf bifurcations, and possible stable/bi-stable spatially inhomogeneous staggered periodic patterns, bi-stable spatially inhomogeneous synchronous periodic patterns, are theoretically predicted. Finally, numerical experiments also support theoretical predictions and partially extend them. In a word, theoretical analyses indicate that, on the one hand, large predator-taxis can eliminate spatial patterns caused by self-diffusion; on the other hand, the joint effects of predator-taxis and conversion time delay can induce complex survival patterns, e.g., bi-stable spatially heterogeneous staggered/synchronous periodic patterns, thus diversify populations' survival patterns.

Received: Added at production | Revised: Added at production | Accepted: Added at production

DOI: xxx/xxxx

RESEARCH ARTICLE

Multi-stable and spatiotemporal staggered patterns in a predator-prey model with predator-taxis and delay†

Yue Xing | Weihua Jiang* | Xun Cao

[1]School of Mathematics, Harbin Institute of Technology, Harbin, 150001, P.R. China

Correspondence
*Weihua Jiang, School of Mathematics, Harbin Institute of Technology, Harbin, 150001, P.R. China. Email: jiangwh@hit.edu.cn

Summary

The effects of predator-taxis and conversion time delay on formations of spatiotemporal patterns in a predator-prey model are explored. Firstly, the well-posedness, which implies global existence of classical solutions, is proved. Then, we establish critical conditions for the destabilization of coexistence equilibrium through Turing/Turing-Turing bifurcations via describing the first Turing bifurcation curve, and theoretically predict possible bi-stable/multi-stable spatially heterogeneous patterns. Next, we demonstrate that coexistence equilibrium can also be destabilized through Hopf, Hopf-Hopf, Turing-Hopf bifurcations, and possible stable/bi-stable spatially inhomogeneous staggered periodic patterns, bi-stable spatially inhomogeneous synchronous periodic patterns, are theoretically predicted. Finally, numerical experiments also support theoretical predictions and partially extend them. In a word, theoretical analyses indicate that, on the one hand, large predator-taxis can eliminate spatial patterns caused by self-diffusion; on the other hand, the joint effects of predator-taxis and conversion time delay can induce complex survival patterns, e.g., bi-stable spatially heterogeneous staggered/synchronous periodic patterns, thus diversify populations' survival patterns.

KEYWORDS:
predator-prey model, pattern formations, Turing bifurcation, Hopf bifurcation, predator-taxis

1 | INTRODUCTION

In recent years, predator-prey model has always been a core topic of concerns in ecology and biomathematics [13,22,23,26,44]. In the real world, besides random movement [7,8,19], the spatial movements of predator and prey may actually be more directional, for example, predator chases prey (prey-taxis) [10,14,24,36], or prey avoids predator (predator-taxis) [35,37,40]. The existing researches about the directed movements of predator and prey, have also provided new insights into the emergence of spatial non-uniform distribution of species [2,21,25,32]. On the other hand, time delay caused by the conversion of predator's capture behavior into predator's growth has also often been taken into account [3,41]. Hence, incorporating chemotaxis and time delay into the classical

†The research is supported by the National Natural Science Foundation of China (No. 11871176).
[0]**MSC Classification:** 35B32, 35K57, 92C15

predator-prey model is necessary and reasonable, and the corresponding model is written as

$$\begin{cases} \frac{\partial u}{\partial t} = \nabla \cdot (d_u \nabla u + \alpha \zeta_1(u) \nabla v) + u f_1(u) - p(u,v)v, & x \in \Omega,\ t > 0, \\ \frac{\partial v}{\partial t} = \nabla \cdot (d_v \nabla v - \eta \zeta_2(v) \nabla u) + c p(u_\tau, v_\tau) v - v f_2(v), & x \in \Omega,\ t > 0, \\ \frac{\partial u}{\partial \vec{n}} = \frac{\partial v}{\partial \vec{n}} = 0, & x \in \partial\Omega, t > 0, \end{cases} \tag{1}$$

with $u_\tau = u(x, t-\tau), v_\tau = v(x, t-\tau)$, and $\Omega \subset \mathbb{R}^n$, $\vec{n}$ is the outer unit normal vector on $\partial\Omega$. $u(x,t)$ and $v(x,t)$ represent the densities of prey and predator at location x and time t respectively, d_u and d_v stand for random dispersal rates of prey and predator respectively, thus are positive, and $c > 0$ reflects the conversion rate. The function $f_1(u)$ describes the growth rate of prey, of which the most common cases are constant growth rate $f_1(u) = r_0 > 0$, logistic growth rate $f_1(u) = r_0(1 - \frac{u}{N})$ with $N > 0$, etc., while $f_2(v)$ describes the mortality of predator, of which the most common cases are constant mortality $f_2(v) = m_1 > 0$, linear mortality $f_2(v) = m_1 + m_2 v$ with $m_2 > 0$, etc. Moreover, $p(u,v)$ is the functional response function, and some common cases are as follows,

$$\text{Holling type II: } p(u,v) = \frac{b_1 u}{b_2 + u},$$
$$\text{Holling type III: } p(u,v) = \frac{b_1 u^2}{b_2 + u^2},$$
$$\text{ratio-dependent: } p(u,v) = \frac{b_1 u}{b_2 v + u},$$

with $b_1 > 0,\ b_2 > 0$. In particular, time delay $\tau \geqslant 0$ is regarded as the contribution of the predation occurred in the past to the current growth of predator[18,28]. $\nabla \cdot (\alpha \zeta_1(u) \nabla v)$ describes the movement of prey toward a lower density of predator, while $-\nabla \cdot (\eta \zeta_2(u) \nabla v)$ describes the movement of predator toward a higher density of prey, where $\alpha,\ \eta \geqslant 0$ are chemotaxis coefficients, and the sensitivity function $\zeta_1(u)$ can be chosen as[34], e.g.,

$$\text{linear: } \zeta_1(u) = u,$$
$$\text{Ricker: } \zeta_1(u) = u e^{-\epsilon u},$$
$$\text{saturated: } \zeta_1(u) = \frac{u}{1 + \epsilon u^m},$$

with $\epsilon > 0,\ m \geqslant 1$, and $\zeta_2(v)$ can be selected analogously.

For model (1) with $\zeta_1(u) = u,\ \zeta_2(v) = v$ and $\tau = 0$, spatial patterns induced by prey-taxis and predator-taxis have been discussed by Wang et al.[38], and they showed that spatial patterns can be eliminated by large predator-taxis and prey-taxis. The results on Turing instability can be also found in Cao and Wu[5], where sufficient conditions for the emergence of spatial patterns were provided, and the authors further revealed that the appearances of spatial patterns does not necessarily require that self-diffusion rate of predator is greater than that of prey in the presence of chemotaxis.

As for model (1) with only prey-taxis ($\alpha = 0,\ \eta > 0$) and $\tau = 0$, global existence, asymptotic behavior or blow-up of solutions in general parabolic-parabolic systems with prey-taxis have been widely studied, for example, see[33,42] and references therein. Pattern formations induced by prey-taxis with $\zeta_2(v) = v$ have also been discussed in detail in[20] for different $f_1,\ f_2$ and p. Specifically speaking, Lee et. al.[20] showed that large prey-taxis tends to stabilize the coexistence equilibrium when $f_1,\ f_2$ and p correspond to logistic growth rate, constant mortality, and ratio-dependent forms. Moreover, Gao and Guo[9] demonstrated that the local stability of the constant steady state is enhanced by the presence of prey-taxis. Subsequently, Qiu et al.[27] showed that prey-taxis can suppress the globally asymptotical stability of the coexistence steady state, and pointed out that due to the effect of prey-taxis, periodic solutions bifurcating from the coexistence steady state via Hopf bifurcation can be spatially inhomogeneous.

Also, there are some researches on model (1) with only predator-taxis ($\alpha > 0,\ \eta = 0$) and $\tau = 0$, e.g., Wu et al.[35] discussed the general model with predator-taxis and proved that large predator-taxis can make the spatial patterns caused by self-diffusion disappear.

Particularly, when considering that logistic growth rate $f_1(u)$, constant mortality $f_2(v)$, ratio-dependent functional response $p(u,v)$ and linear sensitivity function $\zeta_1(u)$, model (1) reads

$$\begin{cases} \frac{\partial u}{\partial t} = \nabla \cdot (d_u \nabla u + \alpha u \nabla v) + u(x,t)(r_0 - a u(x,t)) - \frac{b_1 u(x,t)}{b_2 v(x,t) + u(x,t)} v(x,t), \\ \frac{\partial v}{\partial t} = \nabla \cdot (d_v \nabla v) - m_1 v(x,t) + \frac{c b_1 u(x,t-\tau)}{b_2 v(x,t-\tau) + u(x,t-\tau)} v(x,t),\ x \in \Omega, t > 0, \\ \frac{\partial u}{\partial \vec{n}} = \frac{\partial v}{\partial \vec{n}} = 0,\ x \in \partial\Omega, t > 0, \\ u(x,t) = u_0(x,t) \geqslant 0,\ v(x,t) = v_0(x,t) \geqslant 0,\ (x,t) \in \Omega \times [-\tau, 0], \end{cases} \tag{2}$$

where $\Omega = (0, \pi)$. r_0 and $\frac{r_0}{a}$ stand for intrinsic growth rate of prey and carrying capacity, respectively, m_1 is mortality of predator, which is independent of its density, b_1 and b_2 denote the capturing rate and half saturation constant, respectively. The initial functions u_0 and v_0 are non-negative, continuous and satisfy

$$(u_0, v_0) \in (W^{1,p}(\Omega \times [-\tau, 0], \mathbb{R}^+))^2, \ p > 1. \tag{3}$$

For model (2) with $\tau = 0$, by replacing $\nabla \cdot (\alpha u \nabla v)$ with $\nabla \cdot (\alpha(1 - \frac{u}{M})u\nabla v)$, Wang and Zou [37] investigated the formations of spatial patterns and found that small predator-taxis can lead to spatial patterns, where M measures the maximum number of prey that a unit volume can accommodate. As for (2) with $\tau = 0$ and a general form of predator-taxis, Gao [12] proved the global existence and uniform boundedness of the classical solutions. For the case with no chemotaxis, that is, for $\alpha = 0$, Song et al. [31] considered the delayed model (2) and discussed the existence and stability of the delay-induced spatially homogeneous periodic orbit.

In this paper, we would like to reveal the diversities of populations' survival patterns caused by predator-taxis and conversion time delay from the perspective of studying Turing bifurcation, Hopf bifurcation, Turing-Turing bifurcation, Turing-Hopf bifurcation and so on for system (2).

Firstly, we prove the well-posedness of (2). Secondly, for system (2) without conversion time delay, we establish conditions for the existences of Turing bifurcation and Turing-Turing bifurcation. Particularly, we describe the first Turing bifurcation curve precisely in (d_u, α)-plane, which is piecewise smooth with the segment points being Turing-Turing bifurcation points. Hence, the latent steady states with different wave frequencies that system (2) may exhibit can be forecasted by virtue of the first Turing bifurcation curve. Compared to [37], we give a larger range of parameters when the stability of the positive constant steady state is broken by Turing bifurcation. Moreover, for system (2), we theoretically reveal that large predator-taxis will suppress the appearance of spatial patterns caused by random diffusion.

Afterwards, the conditions for the existences of Hopf bifurcation and Hopf-Hopf bifurcation are given when considering the effects of conversion time delay. We completely determine the finite range of wave frequencies when Hopf bifurcation occurs in system (2). Especially, by describing the finite Hopf bifurcation curves, we also attain the first Hopf bifurcation curve, and determine the stable periodic solutions with different wave frequencies that system (2) may exhibit intuitively, and show that the positive constant steady state will be destabilized through Hopf-Hopf bifurcation at the segment points. Differing from the most previous studies on reaction-diffusion systems with only self-diffusion, our results show that when the positive constant steady state is destabilized, system (2) will exhibit stable periodic patterns with non-zero wave frequencies through Hopf bifurcation and some abundant periodic patterns through Hopf-Hopf bifurcation, such as transient quasi-periodic patterns and bistable periodic patterns, i.e. two stable periodic patterns with different spatial wave frequencies coexist.

Apart from those, the instability of positive constant steady state may also be brought about by some other bifurcations, such as Turing-Hopf bifurcation, Turing-Turing-Hopf bifurcation, Turing-Hopf-Hopf bifurcation and so on. We also establish the conditions for the existences of the corresponding bifurcations. And it is shown from a numerical perspective that a pair of stable spatially inhomogeneous synchronous time-periodic patterns appear through Turing-Hopf bifurcation.

This paper is organized as follows. Global existence of the classical solutions is given in Section 2. In Section 3 and Section 4, we state the main results about Turing instability and Hopf bifurcation for system (2). Some numerical simulations are also given to illustrate theoretical results. At last, we finish our study with conclusions in Section 5.

Throughout the paper, $\mathbb{N}$ is the set of all positive integers, and $\mathbb{N}_0 = \mathbb{N} \cup \{0\}$. As for the definitions of the mode-k_1 Turing bifurcation and mode-$(k_1, k_1 + 1)$ Turing-Turing bifurcation, as well as mode-k_2 Hopf bifurcation, mode-(k_1, k_2) Turing-Hopf bifurcation, mode-$(k_2, \tilde{k}_2)$ Hopf-Hopf bifurcation and so on, which will be mentioned later, the reader may refer to [6,11,16].

2 | GLOBAL EXISTENCE OF THE CLASSICAL SOLUTIONS

Before starting to formally investigate the long-term dynamics, we first prove the well-posedness of system (2), and the result is inspired by [29].

Theorem 1. System (2) admits a unique and positive classical solution $(u, v) \in (C((0, \infty), W^{1,p}(\Omega \times [-\tau, 0], \mathbb{R}^+)) \cap C^{2,1}((0, \infty) \times \overline{\Omega}, \mathbb{R}^+))^2$ with $p > 1$, if the initial values satisfy (3).

Proof. When $\tau = 0$, it follows [12] that the conclusion is valid.

When $\tau > 0$, for $0 \leqslant t \leqslant \tau$, from the first (second) equation of (2) and the comparison principle for parabolic equations, we have $u \geqslant 0$ ($v \geqslant 0$). Further by [39], we have $u > 0$ ($v > 0$) for $0 \leqslant t \leqslant \tau$. Moreover, it follows from [1] that (2) has a unique classical

solution $(C((0,T),W^{1,p}(\Omega\times[-\tau,0],\mathbb{R}^+))\cap C^{2,1}((0,T)\times\overline{\Omega},\mathbb{R}^+))^2$. Noting that

$$G_1(u,v)\triangleq r_0-au-\frac{b_1v}{b_2v+u}\leqslant r_0,$$
$$G_2(u_\tau,v_\tau)\triangleq\frac{cb_1u_\tau}{b_2v_\tau+u_\tau}-m_1\leqslant cb_1,$$

the classical solution can be extended to $t\in[0,\tau]$ and $(u,v)\in(C((0,\tau),W^{1,p}(\Omega\times[-\tau,0],\mathbb{R}^+))\cap C^{2,1}((0,\tau)\times\overline{\Omega},\mathbb{R}^+))^2$. Now by repeating the above proof for $t\in[\tau,2\tau]$ and $t\in[n\tau,(n+1)\tau]$ $(n\geqslant 2)$, we have the analogous results. Thus, the global existence of the classical positive solution of (2) can be obtained, which is obviously positive. □

3 | TURING INSTABILITY AND MULTI-STABLE SPATIAL PATTERNS

Firstly, we analyze the existence and stability of positive constant steady state for the homogeneous system corresponding to system (2).

In fact, there is a unique positive equilibrium $\bar{E}:=(\bar{u},\bar{v})$ for system (2) if

$$c>\frac{m_1}{b_1}\text{ and }r_0>\frac{cb_1-m_1}{cb_2},\tag{4}$$

where

$$\bar{u}=\frac{1}{a}(r_0-\frac{cb_1-m_1}{b_2ac}),\ \bar{v}=\frac{cb_1-m_1}{m_1b_2}\bar{u}.$$

Then, the linearized equations of system (2) at $\bar{E}$ are given by

$$\begin{cases}u_t=d_u\frac{\partial^2}{\partial x^2}u+\alpha\bar{u}\frac{\partial^2}{\partial x^2}v+(-a\bar{u}+\frac{b_1\bar{u}\bar{v}}{(b_2\bar{v}+\bar{u})^2})u-\frac{b_1\bar{u}^2}{(b_2\bar{v}+\bar{u})^2}v,\\ v_t=d_v\frac{\partial^2}{\partial x^2}v+\frac{cb_1b_2\bar{v}^2}{(b_2\bar{v}+\bar{u})^2}u_\tau-\frac{cb_1b_2\bar{u}\bar{v}}{(b_2\bar{v}+\bar{u})^2}v_\tau,\\ u_x(0,t)=v_x(0,t)=0,\ u_x(\pi,t)=v_x(\pi,t)=0.\end{cases}\tag{5}$$

Let $\{\mu_k=k^2:k\in\mathbb{N}_0\}$ be the eigenvalues of operator $-\frac{\partial^2}{\partial x^2}$ on $(0,\pi)$ subject to Neumann boundary conditions. And for the sake of convenience, denote

$$\varpi:=\frac{m_1(cb_1-m_1)}{c^2b_1b_2}>0,$$

then the characteristic equations of (5) read

$$D_k(\lambda,\tau,\alpha):=\lambda^2+p_k\lambda+\sigma_k+(s_k\lambda+q_k(\alpha))e^{-\lambda\tau}=0,\quad k\in\mathbb{N}_0,\tag{6}$$

where

$$\begin{aligned}p_k&=k^2(d_u+d_v)+(a\bar{u}-\varpi),\\ s_k&=cb_2\varpi,\\ \sigma_k&=k^4d_ud_v+k^2d_v(a\bar{u}-\varpi),\\ q_k(\alpha)&=k^2cb_2\bar{v}\varpi\alpha+cb_2\varpi(k^2d_u+a\bar{u}).\end{aligned}\tag{7}$$

For $\tau=0$, (6) turns into

$$D_k(\lambda,0,\alpha)=\lambda^2+(p_k+s_k)\lambda+(\sigma_k+q_k(\alpha))=0,\quad k\in\mathbb{N}_0.\tag{8}$$

Denote $DET_k:=\sigma_k+q_k(\alpha)$, $TR_k:=-(p_k+s_k)$ for $k\in\mathbb{N}_0$, then

$$\begin{aligned}DET_k&=k^4d_ud_v+k^2[d_v(a\bar{u}-\varpi)+d_ucb_2\varpi+\alpha cb_2\bar{v}\varpi]+acb_2\bar{u}\varpi,\\ TR_k&=-k^2(d_u+d_v)-(a\bar{u}-\varpi)-cb_2\varpi.\end{aligned}$$

If

$$c>\frac{m_1}{b_1}\text{ and }r_0>\underline{r_0}\triangleq\max\left\{\frac{cb_1-m_1}{cb_2},\frac{(cb_1-m_1)(cb_1+m_1-cb_2m_1)}{c^2b_1b_2}\right\},\tag{9}$$

then $TR_0<0$, hence $\bar{E}$ is locally asymptotically stable for local ODE system since $DET_0>0$. So in the following discussions, we always assume that (9) is satisfied.

Next, we devote ourselves to discussing the occurrences of Turing bifurcation for system (2).

For convenience, denote

$$\bar{r}_0 := \frac{(cb_1 - m_1)(cb_1 + m_1)}{c^2 b_1 b_2} > 0,$$

and it is obvious that $\bar{r}_0 > \underline{r_0}$.

When $r_0 \geqslant \bar{r}_0$, then $a\bar{u} - \varpi \geqslant 0$, hence $TR_k < 0$, $DET_k > 0$ for $k \in \mathbb{N}_0$, which indicates that $\bar{E}$ is locally asymptotically stable.

When $r_0 < \bar{r}_0$, then $a\bar{u} - \varpi < 0$. According to (9), $TR_k < 0$ for $k \in \mathbb{N}_0$ also holds. Whereas, there exists some $k \in \mathbb{N}$ such that $DET_k < 0$, meaning that Turing bifurcation can occur for system (2). Then, for any fixed $d_v > 0$, define

$$\alpha(k, d_u) := -\frac{d_u d_v k^4 + (d_v(a\bar{u} - \varpi) + d_u c b_2 \varpi)k^2 + acb_2\bar{u}\varpi}{k^2 c b_2 \bar{v}\varpi},\ d_u > 0,\ k \in \Lambda, \tag{10}$$

where

$$\Lambda := \left\{ k \in \mathbb{N} : k > \hat{k} \triangleq \sqrt{\frac{acb_2\bar{u}\varpi}{d_v(\varpi - a\bar{u})}} \right\}. \tag{11}$$

Also, denote

$$\bar{\alpha}(k) := \lim_{d_u \to 0^+} \alpha(k, d_u) = -\frac{a\bar{u}}{k^2\bar{v}} + \frac{d_v(\varpi - a\bar{u})}{cb_2\bar{v}\varpi}. \tag{12}$$

Then, to describe the critical conditions for the instability of the positive equilibrium, we first discuss the monotonicity of $\bar{\alpha}(k)$ with respect to the wave number k.

Lemma 2. For any $a, b_1, b_2, m_1, d_v > 0$, provided that $c > \frac{m_1}{b_1}$, $\underline{r_0} < r_0 < \bar{r}_0$, then $\bar{\alpha}(k) > 0$ is monotonically increasing in k for $k \in \Lambda$.

A direct calculation from $\alpha(k, d_u) = 0$ yields

$$d_u^k := -\frac{d_v(a\bar{u} - \varpi)k^2 + acb_2\bar{u}\varpi}{k^2(d_v k^2 + cb_2\varpi)},\ k \in \Lambda, \tag{13}$$

which is a critical value of d_u when $\bar{E}$ is destabilized.

For any $d_v > 0$, let

$$\bar{k} := \begin{cases} \lfloor k_* \rfloor + 1, & \text{for } d_u^{\lfloor k_* \rfloor} \leqslant d_u^{\lfloor k_* \rfloor + 1}, \\ \lfloor k_* \rfloor, & \text{for } d_u^{\lfloor k_* \rfloor} > d_u^{\lfloor k_* \rfloor + 1}, \end{cases} \tag{14}$$

then $\bar{k}$ is the critical wave number of the nonconstant steady states arising from $\bar{E}$ through Turing instability, where

$$k_* = \sqrt{\frac{cb_2\varpi(a\bar{u} + \sqrt{a\bar{u}\varpi})}{d_v(\varpi - a\bar{u})}}, \tag{15}$$

and $\lfloor \cdot \rfloor$ is the floor function.

The next lemma concerns the monotonicity of d_u^k in k and $\alpha(k, d_u)$ in d_u, respectively, that is,

Lemma 3. For any $a, b_1, b_2, m_1, d_v > 0$, provided that $c > \frac{m_1}{b_1}$, $\underline{r_0} < r_0 < \bar{r}_0$, then

(i) d_u^k is monotonically increasing with respect to $k \in \mathbb{N}$ for $\hat{k} < k < \bar{k}$, and monotonically decreasing with respect to $k \in \mathbb{N}$ for $k \geqslant \bar{k}$.

(ii) for any $k \in \Lambda$, $\alpha(k, d_u)$ is linear and monotonically decreasing with respect to d_u for $d_u > 0$. Particularly, $\alpha(k, d_u) > 0$ for $0 < d_u < d_u^k$, $k \in \Lambda$.

Proof. We only prove the case of $d_u^{\lfloor k_* \rfloor} \leqslant d_u^{\lfloor k_* \rfloor + 1}$, $\bar{k} = \lfloor k_* \rfloor + 1$, and the other cases can be proved by following the similar arguments.

For part (i), define $\Theta_1(x)$ by

$$\Theta_1(x) := -\frac{d_v(a\bar{u} - \varpi)x + acb_2\bar{u}\varpi}{x(d_v x + cb_2\varpi)},\ x > 0.$$

So by a direct calculation, there exists $x^* = k_*^2$ satisfying that $\Theta_1(x)$ is increasing in x on $(0, x^*)$, and decreasing in x on (x^*, ∞). And by (11), it follows that

$$k_*^2 - \hat{k}^2 = \frac{cb_2\varpi\sqrt{a\bar{u}\varpi}}{d_v(\varpi - a\bar{u})} > 0,$$

that is, $k_* > \hat{k}$, thus $\lfloor k_* \rfloor + 1 \geqslant k_* > \hat{k}$, which implies that d_u^k is decreasing for $\lfloor k_* \rfloor + 1 \leqslant k \in \mathbb{N}$. On the other hand, for $k \in \{k \in \mathbb{N} : \hat{k} < k < \lfloor k_* \rfloor + 1\}$, d_u^k is monotonically increasing with respect to k.

For part (ii), for any $k \in \Lambda$, we rewrite the expression of $\alpha(k, d_u)$ in (10) as follows

$$\alpha(k, d_u) := -\frac{d_v k^2 + cb_2\varpi}{cb_2\bar{v}\varpi} d_u - \frac{d_v(a\bar{u} - \varpi)k^2 + acb_2\bar{u}\varpi}{k^2 cb_2\bar{v}\varpi},\ d_u > 0,$$

then $\alpha(k, d_u)$ is a linear function of d_u, thus for $d_u > 0$, $\alpha(k, d_u)$ is monotonically decreasing with respect to d_u, implying that $\alpha(k, d_u) > 0$ for $0 < d_u < d_u^k$, $k \in \Lambda$.

□

As required by the model background, we focus on the case where the predator-taxis coefficient is non-negative. To this end, for any $d_v > 0$, define

$$\alpha_*(k, d_u) := \max\{\alpha(k, d_u), 0\},\ k \in \Lambda,\ 0 < d_u < d_u^{\bar{k}}. \tag{16}$$

It is well known that the first critical value of Turing bifurcation determines the stability of positive constant steady state [15]. So to describe the critical region where the stability of $\bar{E}$ changes in (d_u, α)-plane, next we discuss the intersections of $\alpha = \alpha_*(k, d_u)$ for $k \in \Lambda, 0 < d_u < d_u^{\bar{k}}$.

Lemma 4. For any $a, b_1, b_2, m_1, d_v > 0$, provided that $c > \frac{m_1}{b_1}$, $\underline{r_0} < r_0 < \bar{r}_0$, then for any $k \in \Lambda$,

(i) the equation

$$\alpha_*(k, d_u) = \alpha_*(k+1, d_u),\ 0 < d_u < d_u^{\bar{k}}$$

has a unique root $d_u^{k,k+1} \in (0, d_u^{k+1})$, which is denoted by

$$d_u^{k,k+1} := \frac{acb_2\bar{u}\varpi}{d_v k^2(k+1)^2}. \tag{17}$$

(ii) for $k \geqslant \bar{k}$,

$$\begin{aligned} &\alpha_*(k, d_u) > \alpha_*(k+1, d_u) \geqslant \alpha_*(k+2, d_u) \geqslant \cdots, \\ &\alpha_*(k, d_u) > \alpha_*(k-1, d_u) > \alpha_*(k-2, d_u) > \cdots > \alpha_*(\bar{k}, d_u), \end{aligned} \tag{18}$$

for $d_u^{k,k+1} < d_u < d_u^{k-1,k}$, where $d_u^{\bar{k}-1,\bar{k}} := d_u^{\bar{k}}$.

(iii) for $\hat{k} < k < \bar{k}$

$$\alpha_*(\bar{k}, d_u) \geqslant \alpha_*(\bar{k}-1, d_u) \geqslant \cdots \geqslant \alpha_*(\lfloor \hat{k} \rfloor + 1, d_u),\ \text{for } 0 < d_u < d_u^{\bar{k}}. \tag{19}$$

Proof. The part (i) is obvious. As for parts (ii) and (iii), below we only give the proof when $d_u^{\lfloor k_* \rfloor} \leqslant d_u^{\lfloor k_* \rfloor + 1}$, $\bar{k} = \lfloor k_* \rfloor + 1$, and the other cases can be proved similarly.

For part (ii), if $k \geqslant \bar{k}$, then for the first sequence, if further $d_u > d_u^{k,k+1}$, it follows that

$$\alpha_*(k, d_u) - \alpha_*(k+1, d_u) = \frac{(2k+1)(d_u d_v k^2(k+1)^2 - acb_2\bar{u}\varpi)}{cb_2\bar{v}\varpi k^2(k+1)^2} > 0,$$

that is, $\alpha_*(k, d_u) > \alpha_*(k+1, d_u)$. In addition, if $d_u > d_u^{k+1} > d_u^{k,k+1}$, together with the definition of $\alpha_*(k, d_u)$ in (16), then $\alpha_*(k+1, d_u) = \alpha_*(k+2, d_u) = \cdots = 0$, implying that for $d_u > d_u^{k,k+1}$, $\alpha_*(k, d_u) > \alpha_*(k+1, d_u) \geqslant \alpha_*(k+2, d_u) \geqslant \cdots$. Similarly, if $d_u > d_u^{k+1,k+2}$, the $\alpha_*(k+1, d_u) > \alpha_*(k+2, d_u) \geqslant \alpha_*(k+3, d_u) \geqslant \cdots$ holds, and the rest can be done in the same manner. And by (17), $d_u^{\lfloor k_* \rfloor + 1} > d_u^{k,k+1} > d_u^{k+1,k+2} > \cdots > 0$ also holds. Thus, when $d_u > d_u^{k,k+1}$, $\alpha_*(k, d_u) > \alpha_*(k+1, d_u) \geqslant \alpha_*(k+2, d_u) \geqslant \cdots$.

If $d_u < d_u^{k-1,k}$, it analogously follows that

$$\alpha_*(k, d_u) - \alpha_*(k-1, d_u) = \frac{(2k-1)(-d_u d_v k^2(k-1)^2 + acb_2\bar{u}\varpi)}{cb_2\bar{v}\varpi k^2(k-1)^2} > 0,$$

that is, $\alpha_*(k, d_u) > \alpha_*(k-1, d_u)$. So if $d_u < d_u^{k-2,k-1}$, then $\alpha_*(k-1, d_u) > \alpha_*(k-2, d_u)$ and so on. By (17) again, $0 < d_u^{k-1,k} < d_u^{k-2,k-1} < \cdots < d_u^{\lfloor k_* \rfloor + 1}$ holds. Hence, when $d_u < d_u^{k-1,k}$, $\alpha_*(k, d_u) > \alpha_*(k-1, d_u) > \alpha_*(k-2, d_u) > \cdots > \alpha_*(\lfloor k_* \rfloor + 1, d_u)$.

For part (iii), according to Lemma 2 and Lemma 3, if $\hat{k} < k < \bar{k}$, then $\alpha_*(\lfloor k_* \rfloor + 1, d_u) \geqslant \alpha_*(\lfloor k_* \rfloor, d_u) \geqslant \cdots \geqslant \alpha_*(\lfloor \hat{k} \rfloor + 1, d_u)$, $0 < d_u < d_u^{\bar{k}}$. □

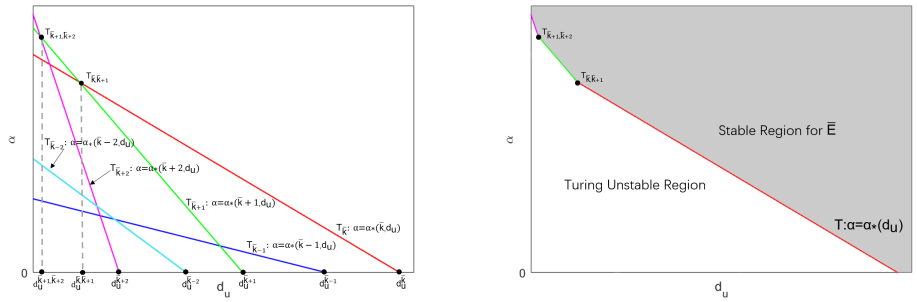

(a) (b)

Figure 1 (a): Turing bifurcation curves $\alpha = \alpha_*(k, d_u)$ when $0 < d_u < d_u^{\bar{k}}$ for different $k \in \Lambda$ in (d_u, α)-plane. (b): The first Turing bifurcation curve $\alpha = \alpha_*(d_u), 0 < d_u < d_u^{\bar{k}}$. The non-smooth points $T_{\bar{k},\bar{k}+1}, T_{\bar{k}+1,\bar{k}+2}, \cdots$ are Turing-Turing bifurcation points.

Synthesizing the above discussions, for $k \in \Lambda$, $0 < d_u < d_u^{\bar{k}}$, define

$$\alpha_*(d_u) := \alpha_*(k, d_u),\ d_u \in [d_u^{k,k+1}, d_u^{k-1,k}),\ k \geqslant \bar{k}, \tag{20}$$

with $\bar{k}$ is defined as in (14). Then

$$\alpha = \alpha_*(d_u),\ 0 < d_u < d_u^{\bar{k}} \tag{21}$$

is called **the first Turing bifurcation curve**, which is the critical curve for Turing instability of $\bar{E}$.

Lemma 5. For any $a, b_1, b_2, m_1, d_v > 0$, provided that $c > \frac{m_1}{b_1}$, $\underline{r_0} < r_0 < \bar{r}_0$, then for any $d_u \in (0, d_u^{\bar{k}})$, there must exist some integer $k_1 \geqslant \bar{k}$ such that $d_u \in [d_u^{k_1,k_1+1}, d_u^{k_1-1,k_1})$. Specifically,

(i) if $d_u \in (d_u^{k_1,k_1+1}, d_u^{k_1-1,k_1})$ and $\alpha = \alpha_*(d_u)$, 0 is a simple root of characteristic equation (8) with $k = k_1$, and the other roots of (8) have strictly negative real parts. Moreover, let $\lambda_1(k_1, 0, \alpha)$ be the root of (8) satisfying $\lambda_1(k_1, 0, \alpha_*(d_u)) = 0$, then

$$\frac{d\lambda_1(k_1, 0, \alpha_*(d_u))}{d\alpha} = \frac{-k_1^2 c b_2 \bar{v}\varpi}{p_{k_1} + s_{k_1}} < 0. \tag{22}$$

(ii) if $d_u = d_u^{k_1,k_1+1}$ and $\alpha = \alpha_*(d_u^{k_1,k_1+1})$, then 0 is a simple root of characteristic equation (8) for both k_1 and $k_1 + 1$, and the other roots of (8) have strictly negative real parts.

Proof. Inspired by the proof of[15], we only give the proof of part (i), and the second assertion can be analogously proved.

Note that in (8), $DET_k = 0$ if and only if $\alpha = \alpha_*(k, d_u)$ for $k \in \Lambda$, $0 < d_u < d_u^{\bar{k}}$. So, for any $k_1 \in \Lambda$, $\lambda_1(k_1, 0, \alpha) = 0$ is always a root of (8) with such k_1 when $\alpha = \alpha_*(k_1, d_u)$. By the definition of $\alpha_*(d_u)$ and $\alpha_*(k, d_u)$, if $d_u \in (d_u^{k_1,k_1+1}, d_u^{k_1-1,k_1})$ and $\alpha = \alpha_*(d_u)$, then 0 is a root of (8) with $k = k_1$. Moreover, it follows

$$\frac{\mathrm{d}D_{k_1}(\lambda, 0, \alpha)}{\mathrm{d}\lambda}\,|_{\lambda=0} = -TR_{k_1} > 0$$

that $\lambda = 0$ is simple. The condition (9) ensures that $TR_k < 0$ for all $k \in \mathbb{N}_0$ and $DET_k > 0$ for $k \geqslant \bar{k}, k \in \mathbb{N}$ and $k \neq k_1$. Thus, all the other roots of (8) have strictly negative real parts. Differentiating (8) with respect to α, the transversality conditions in (22) can be obtained directly. □

In Figure 1 (a), we demonstrate the schematic diagram of Turing bifurcation curves $\alpha = \alpha_*(k, d_u)$ when $0 < d_u < d_u^{\bar{k}}$ for different $k \in \Lambda$ in (d_u, α)-plane to illustrate the properties presented in Lemma 4. The corresponding first Turing bifurcation curve $\alpha = \alpha_*(d_u), 0 < d_u < d_u^{\bar{k}}$ is plotted in Figure 1 (b), and the non-smooth points of $\alpha = \alpha_*(d_u), 0 < d_u < d_u^{\bar{k}}, T_{\bar{k},\bar{k}+1}, T_{\bar{k}+1,\bar{k}+2}$, $\cdots$ are Turing-Turing bifurcation points.

So in summary, we have

Theorem 6. For model (2) with $\tau = 0$ and any $a, b_1, b_2, m_1, d_v > 0$, provided that $c > \frac{m_1}{b_1}$, then

(1) when $r_0 \geqslant \bar{r}_0$, for $d_u > 0, \alpha > 0$, positive constant steady state $\bar{E}$ is always locally asymptotically stable.

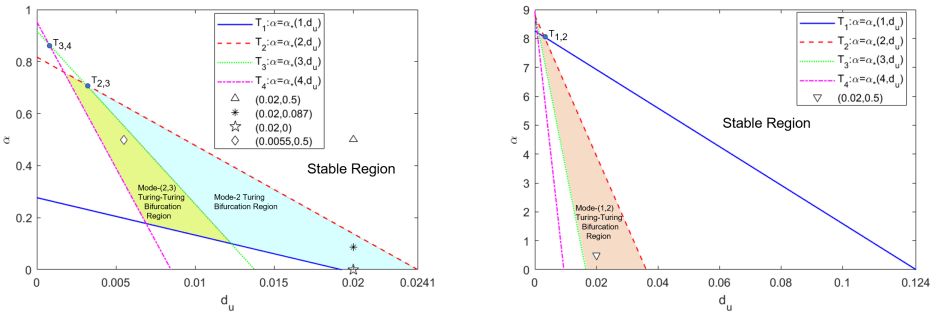

(a) $d_v = 0.2$ (b) $d_v = 1.8$

Figure 2 Stable region, Turing bifurcation region and Turing-Turing bifurcation region for $d_v = 0.2,\ 1.8$, respectively.

(2) when $\underline{r_0} < r_0 < \bar{r}_0$,

(a) if further $d_u \geqslant d_u^{\bar{k}}$, the $\bar{E}$ is locally asymptotically stable for $\alpha > 0$.

(b) when $0 < d_u < d_u^{\bar{k}}$,

(i) $\bar{E}$ is locally asymptotically stable for $\alpha > \alpha_*(d_u)$, and unstable for $0 < \alpha < \alpha_*(d_u)$.

(ii) if further $d_u \in (d_u^{k_1,k_1+1}, d_u^{k_1-1,k_1})$ for some $k_1 \geqslant \bar{k}$ and $k_1 \in \mathbb{N}$, (2) undergoes mode-k_1 Turing bifurcation when $\alpha = \alpha_*(d_u)$.

(iii) if further $d_u = d_u^{k_1,k_1+1}$ for some $k_1 \geqslant \bar{k}$ and $k_1 \in \mathbb{N}$, (2) undergoes mode-(k_1, k_1+1) Turing-Turing bifurcation when $\alpha = \alpha_*(d_u^{k_1,k_1+1})$.

Remark 1. **(Turing patterns and Turing-Turing patterns)** Note that sufficient conditions for the formations of spatial patterns have been provided in[37], while the condition $0 < \alpha < \alpha_*(d_u),\ 0 < d_u < d_u^{\bar{k}}$ given in Theorem 6 is not only sufficient but also necessary for pattern formations.

As shown in Figure 1 (b), the first Turing bifurcation curve $\alpha = \alpha_*(d_u),\ 0 < d_u < d_u^{\bar{k}}$, is formed by connecting Turing bifurcation curves of mode-$\bar{k}$, mode-$\bar{k}+1$, mode-$\bar{k}+2$, $\cdots$ with Turing-Turing bifurcation points $T_{\bar{k},\bar{k}+1}$, $T_{\bar{k}+1,\bar{k}+2}$, $\cdots$, which indicates that the positive constant steady state can be destabilized by mode-k Turing bifurcation, thus system (2) will harvest the spatially inhomogeneous steady states shaped like $\cos kx$, and also suggests that the positive constant steady state can be destabilized by mode-$(k, k+1)$ Turing-Turing bifurcation, thus system (2) will harvest more complex spatial patterns, such as multiple superposition solutions of $\cos kx$ and $\cos(k+1)x$, or the coexistence of multi-stable spatial patterns shaped like $\cos kx$ and shaped like $\cos(k+1)x$, where the possible values of k are $\bar{k}, \bar{k}+1, \cdots$.

Moreover, it can be concluded that large predator-taxis has the effects of eliminating spatial patterns which arise due to random dispersal of predator and prey. Besides, it follows from Lemma 3 and (20) that $\alpha = \alpha_*(d_u)$ is decreasing with respect to d_u for $0 < d_u < d_u^{\bar{k}}$, which means that when the self-diffusion d_u of prey is small, the heterogeneity of spatial distributions of the two populations can be eliminated by increasing the predator-taxis coefficient α, that is to say, large predator-taxis can supplement small self-diffusion of prey.

Next, we provide some examples to intuitively explain the above theoretical analysis.

Here we refer to parameter selections in[30], and let

$$a = 0.4902,\ r_0 = 0.5,\ c = b_1 = 1$$
$$b_2 = 0.9804,\ m_1 = 0.6,\ \tau = 0.$$

Then (9) is satisfied, thus $\bar{E} = (0.1877, 0.1276)$ is locally asymptotically stable for local ODE system.

Further, when $d_v = 0.2,\ 1.8$, respectively, Turing bifurcation sets are given in Figure 2, where $\alpha = \alpha_*(k, d_u)$ for $k = 1, 2, 3, 4, \cdots$ are Turing bifurcation curves, and the regions where multiple spatial patterns exist are marked. For ease of citations, stable regions are denoted as D, mode-2 Turing bifurcation region is denoted as D_2, and mode-$(1,2)$, mode-$(2,3)$ Turing-Turing bifurcation regions are denoted as $D_{1,2},\ D_{2,3}$, respectively.

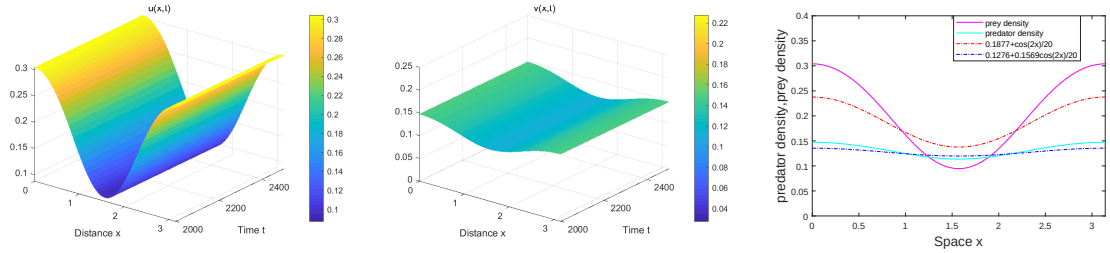

(a) $(d_u, \alpha) = (0.02, 0)$

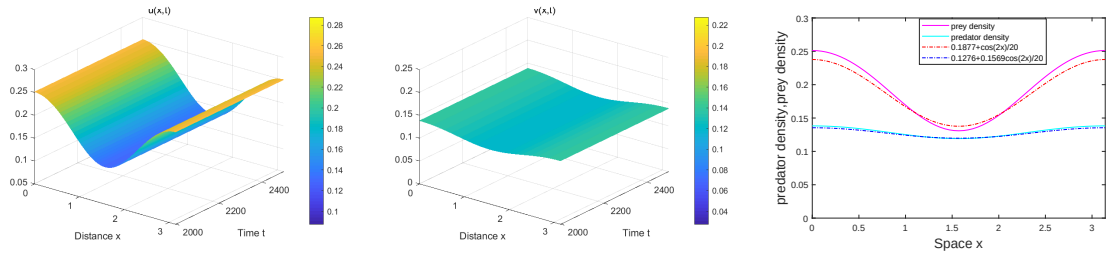

(b) $(d_u, \alpha) = (0.02, 0.087)$

Figure 3 The spatial distributions of the two populations are inhomogeneous when $(d_u, \alpha) = (0.02, 0)$ and $(d_u, \alpha) = (0.02, 0.087)$, respectively.

Example 1. (Turing bifurcation and spatial patterns)

Let $d_v = 0.2$, we want to show the effects of predator-taxis on pattern formations.

It follows from (14) that $\bar{k} = 2$. Due to (13), $d_u^{\bar{k}} = d_u^2 = 0.0241$. And by (17), $d_u^{2,3} = 0.0031$.

When $d_u \in (d_u^{2,3}, d_u^2)$, Theorem 6 indicates that system (2) undergoes mode-2 Turing bifurcation at $\alpha = \alpha_*(d_u)$. And the eigenfunction corresponding to the eigenvalue μ_2 is

$$(\bar{u} + \cos 2x, \bar{v} + \frac{cb_1b_2\bar{v}^2}{\mu_2 d_v(b_2\bar{v} + \bar{u})^2 + cb_1b_2\bar{u}\bar{v}} \cos 2x)^T = (\bar{u} + \cos 2x, \bar{v} + 0.1569 \cos 2x)^T. \tag{23}$$

Bifurcation theory indicates that when $(d_u, \alpha) \in D_2$, there will be spatially inhomogeneous patterns and the waveforms are consistent with those of eigenfunctions given by (23).

(1) Let $d_u = 0.02$, then $\alpha_*(0.02) = 0.1384$. Let $\alpha = 0 < \alpha_*(0.02)$ and $\alpha = 0.087 < \alpha_*(0.02)$ respectively, then $(d_u, \alpha) \in D_2$ (see Figure 2 (a)). Thus, mode-2 Turing bifurcation occurs and $\bar{E}$ becomes unstable. Meanwhile, spatially inhomogeneous patterns shaped like $\cos 2x$ are theoretically expected to appear. Specifically, when choosing $(0.1877+0.1 \cos 2x, 0.1276+0.1 \cos 2x)$ as initial values, numerical results are presented in Figure 3, and the third column of Figure 3 illustrates that the waveforms of spatially inhomogeneous patterns are consistent with the waveforms of corresponding eigenfunction given by (23).

(2) If we further choose a larger predator-taxis coefficient $\alpha = 0.5 > \alpha_*(0.02) = 0.1384$, then $(d_u, \alpha) \in D$ (see Figure 2 (a)). Thus $\bar{E}$ is locally asymptotically stable. Let $(0.1877 + 0.1 \cos 2x, 0.1276 + 0.1 \cos 2x)$ be initial values, and numerical results are presented in Figure 4.

Consequently, it is numerically confirmed that large predator-taxis has effects on eliminating spatial patterns resulting from self-diffusion by comparing Figure 3 with Figure 4.

Example 2. (Turing-Turing bifurcation and multi-stable spatial patterns)

(1) Let $d_v = 0.2$. Compared with Example 1 (2), we further choose a smaller self-diffusion coefficient of prey $d_u = 0.0055$. It follows (13), (16) and (17), that

$$\alpha_*(2, d_u) = 0.6308, \ \alpha_*(3, d_u) = 0.5513, \ \alpha_*(4, d_u) = 0.3310,$$
$$d_u^2 = 0.0241, \qquad d_u^3 = 0.0138, \qquad d_u^{2,3} = 0.0033,$$

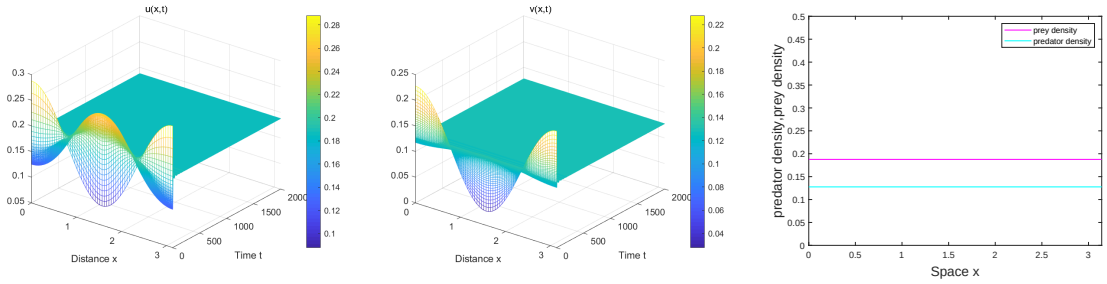

(a) (b) (c)

Figure 4 The spatial distributions of the two populations are homogeneous when $(d_u, \alpha) = (0.02, 0.5)$.

Table 1 Formations and comparisons of multiple spatial patterns.

Case	d_v	(d_u, α)	Figures	Spatial Patterns
I	0.2	$(0.02, 0)$	3 (a)	Spatial patterns with wave frequency 2
		$(0.02, 0.087)$	3 (b)	Spatial patterns with wave frequency 2
II	0.2	$(0.02, 0.5)$	4	Spatially homogeneous patterns
III	0.2	$(0.0055, 0.5)$	5 (a) (b)	Multi-stable spatial patterns with
			5 (c) (d)	wave frequencies 2 and 3
IV	1.8	$(0.02, 0.5)$	6 (a) (b)	Multi-stable spatial patterns with
			6 (c) (d)	wave frequencies 1 and 2

thus $d_u \in (d_u^{2,3}, d_u^3)$ and $(d_u, \alpha) \in D_{2,3}$, that is, (d_u, α) is selected in mode-$(2, 3)$ Turing-Turing bifurcation region (see Figure 2 (a)), where superposition patterns of $\cos 2x$ and $\cos 3x$ or multi-stable spatial patterns shaped like $\cos 2x$ and $\cos 3x$ are theoretically expected to emerge. When we choose $(0.1877 + 0.1\cos 2x, 0.1276 + 0.1\cos 2x)$, $(0.1877 - 0.1\cos 2x, 0.1276 - 0.1\cos 2x)$, $(0.1877 + 0.1\cos 3x, 0.1276 + 0.1\cos 3x)$ and $(0.1877 - 0.1\cos 3x, 0.1276 - 0.1\cos 3x)$ as initial values respectively, as shown in Figure 5, a pair of spatially inhomogeneous patterns with wave frequency 2 and a pair of spatially inhomogeneous patterns with wave frequency 3 coexist, which are multi-stable spatial patterns.

(2) Let $d_u = 0.02$. Compared with Example 1 (2), we further choose a bigger self-diffusion coefficient of predator $d_v = 1.8$. It follows (13), (16) and (17), that

$$\alpha_*(1, d_u) = 6.9267,\ \alpha_*(2, d_u) = 3.9413,\ \alpha_*(3, d_u) = 0,$$
$$d_u^1 = 0.124, \qquad d_u^2 = 0.0362, \qquad d_u^{1,2} = 0.0033,$$

thus $d_u \in (d_u^{1,2}, d_u^2)$ and $(d_u, \alpha) \in D_{1,2}$, that is, (d_u, α) is selected in mode-$(1, 2)$ Turing-Turing bifurcation region (see Figure 2 (b)), where superposition patterns of $\cos x$ and $\cos 2x$ or multi-stable spatial patterns shaped like $\cos x$ and $\cos 2x$ are theoretically expected to emerge. When we choose $(0.1877 + 0.1\cos x, 0.1276 + 0.1\cos x)$, $(0.1877 - 0.1\cos x, 0.1276 - 0.1\cos x)$, $(0.1877 + 0.2\cos 2x, 0.1276 + 0.1\cos 2x)$ and $(0.1877 - 0.2\cos 2x, 0.1276 - 0.1\cos 2x)$ as initial values respectively, as shown in Figure 6, a pair of spatially inhomogeneous patterns with wave frequency 1 and a pair of spatially inhomogeneous patterns with wave frequency 2 coexist, which are multi-stable spatial patterns.

Consequently, the results of Example 2 show that, on the one hand, the positive constant steady state can be destabilized through Turing-Turing bifurcation, resulting in multi-stable spatial patterns. On the other hand, by comparing the results of Figure 5 and Figure 6 with those of Figure 4, respectively, it is numerically illustrated that either small self-diffusion for prey or large self-diffusion for predator will promote spatial patterns to appear, which suggests that predator-taxis can balance the spatial heterogeneity caused by self-diffusion.

For convenience, we summarize the results of Example 1 and Example 2 in Table 1 and make the following comparisons.

The comparison of cases I and II shows that large predator-taxis can eliminate spatial patterns caused by self-diffusion, that is to say, the more sensitive prey is to predation (large predator-taxis), the more evenly distributed the two populations are.

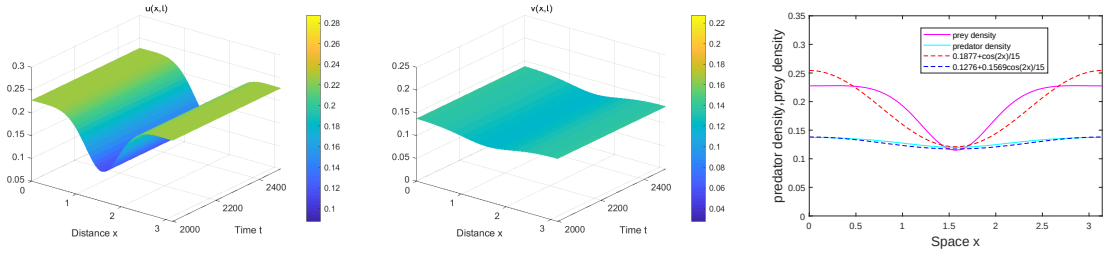

(a) The initial values are $u_0 = 0.1877 + 0.1\cos 2x$, $v_0 = 0.1276 + 0.1\cos 2x$

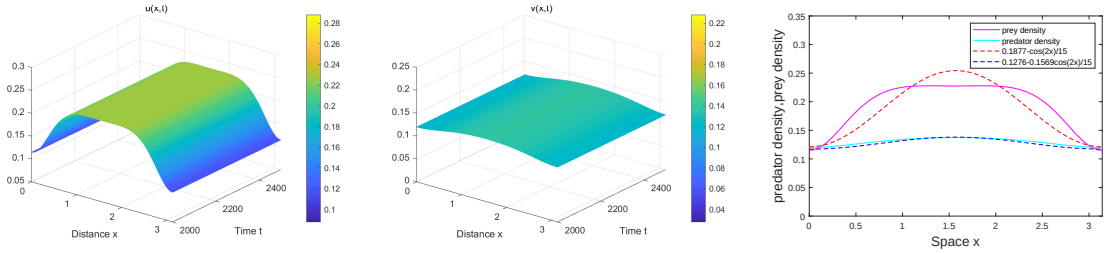

(b) The initial values are $u_0 = 0.1877 - 0.1\cos 2x$, $v_0 = 0.1276 - 0.1\cos 2x$

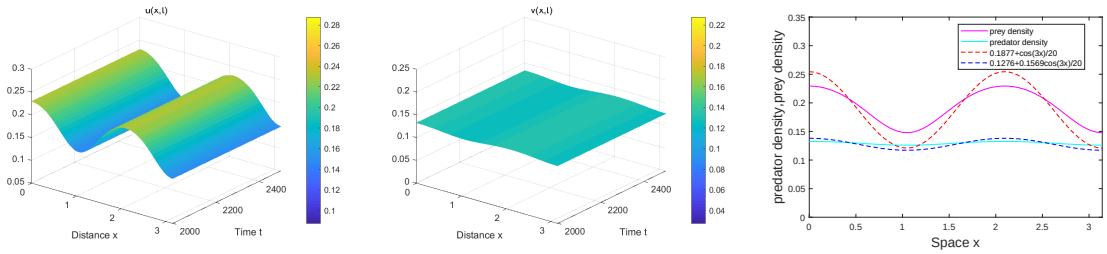

(c) The initial values are $u_0 = 0.1877 + 0.1\cos 3x$, $v_0 = 0.1276 + 0.1\cos 3x$

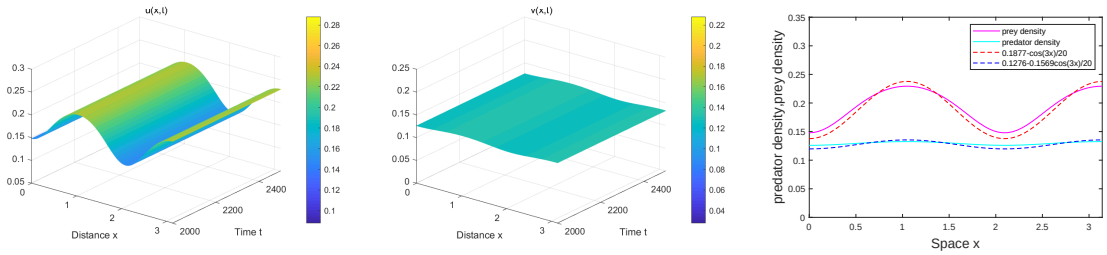

(d) The initial values are $u_0 = 0.1877 - 0.1\cos 3x$, $v_0 = 0.1276 - 0.1\cos 3x$

Figure 5 Multi-stable spatial patterns when $(d_u, \alpha) = (0.0055, 0.5)$. The first two columns are spatial distribution patterns of the two populations shaped like $\cos 2x$ and $\cos 3x$ when different initial values are selected, and the third column is the comparison of shapes of spatial distribution patterns and shapes of the eigenfunctions.

Beyond that, a reasonable phenomenon is explained, that is, when only self-diffusion is considered, fast predator dispersal leads to the appearance of spatial patterns, which will eventually disappear when further considering the chemotaxis behavior of prey avoiding predator, suggesting that predator-taxis can partially cancel out the non-uniform advantage caused by self-diffusion of predator.

The comparison of cases II and III shows that spatial patterns still exist as long as the self-diffusion of prey is small enough. From another perspective, it also shows that predator-taxis and self-diffusion of prey are complementary, that is, predator-taxis is equivalent to accelerating the self-diffusion of prey, and the spatial distributions of the two populations will finally reach homogeneity if predator-taxis is large enough.

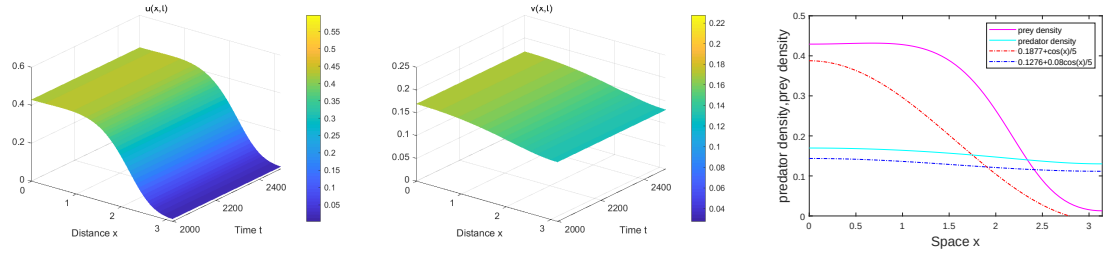

(a) The initial values are $u_0 = 0.1877 + 0.1\cos x$, $v_0 = 0.1276 + 0.1\cos x$

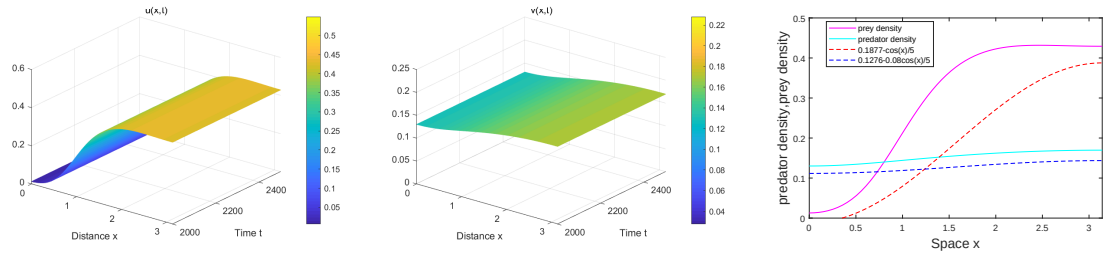

(b) The initial values are $u_0 = 0.1877 - 0.1\cos x$, $v_0 = 0.1276 - 0.1\cos x$

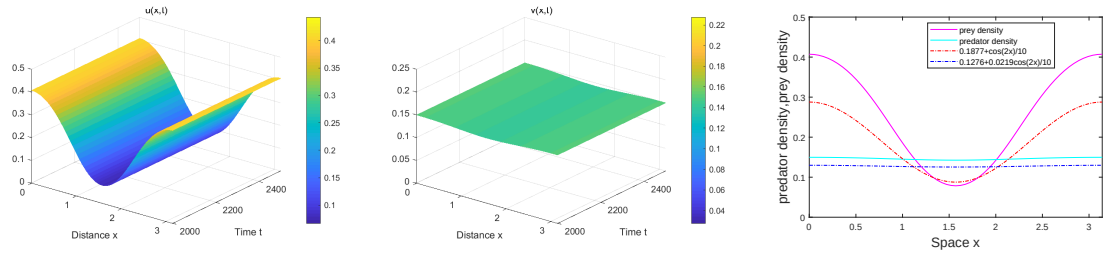

(c) The initial values are $u_0 = 0.1877 + 0.2\cos 2x$, $v_0 = 0.1276 + 0.1\cos 2x$

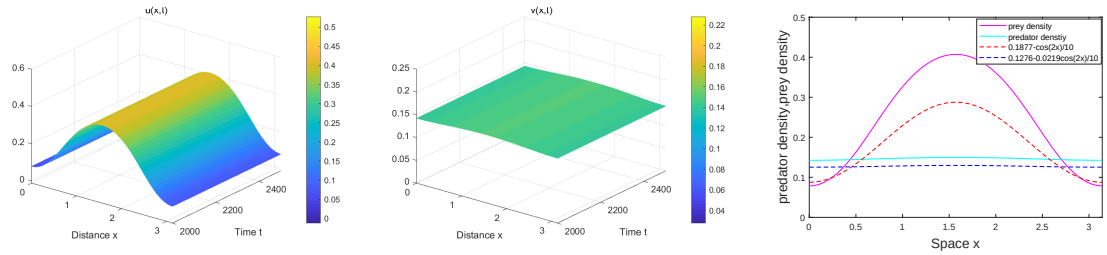

(d) The initial values are $u_0 = 0.1877 - 0.2\cos 2x$, $v_0 = 0.1276 - 0.1\cos 2x$

Figure 6 Multi-stable spatial patterns when $d_v = 1.8$ and $(d_u, \alpha) = (0.02, 0.5)$. The first two columns are spatial distribution patterns of the two populations shaped like $\cos x$ and $\cos 2x$ when different initial values are selected, and the third column is the comparison of shapes of spatial distribution patterns and shapes of the eigenfunctions.

The comparison of cases II and IV shows that the spatial patterns still exist as long as the self-diffusion of predator is large enough. From another perspective, the accelerated self-diffusion of predator is equivalent to the weakened ability of prey to avoid the risk of being preyed, thus increasing the probability of emergence of spatial inhomogeneous patterns.

Case III and Case IV show that spatial inhomogeneous steady states with different wave frequencies can coexist, which in turn indicates that the constant stationary can be destabilized by Turing-Turing bifurcation, thus giving rise to multi-stable spatial patterns.

4 | HOPF BIFURCATION AND SPATIOTEMPORAL STAGGERED PERIODIC PATTERNS

In this part, we discuss the effects of time delay on the stability of the positive constant steady state of system (2).

First, the following result concerning the nonoccurence of Hopf bifurcation for system (2) with $\tau = 0$ holds.

Theorem 7. For model (2) with $\tau = 0$ and $a, b_1, b_2, m_1, d_v > 0$, provided that $c > \frac{m_1}{b_1}$, $r_0 > \underline{r_0}$, then for $d_u, \alpha > 0$, there is no Hopf bifurcation.

Next, we establish the conditions for the occurrence of Hopf bifurcation for system (2) with $\tau > 0$.

Let $\lambda = \pm \mathrm{i}\omega_k(\alpha)$ with $\omega_k(\alpha) > 0$, be a pair of purely imaginary roots of (6). For the sake of convenience, denote $\omega_k(\alpha) \triangleq \omega_k$. Then, for $k \in \mathbb{N}_0$,

$$\begin{aligned} D_k(\mathrm{i}\omega_k, \tau, \alpha) = \sigma_k - \omega_k^2 + q_k(\alpha)\cos(\omega_k\tau) + s_k\omega_k \sin(\omega_k\tau) \\ + \mathrm{i}[p_k\omega_k + s_k\omega_k\cos(\omega_k\tau) - q_k(\alpha)\sin(\omega_k\tau)] = 0. \end{aligned} \tag{24}$$

Separating the real and imaginary parts yields

$$\begin{aligned} \sin(\omega_k\tau) &= \frac{s_k\omega_k(\omega_k^2 - \sigma_k) + p_k q_k(\alpha)\omega_k}{s_k^2\omega_k^2 + q_k(\alpha)^2}, \\ \cos(\omega_k\tau) &= \frac{q_k(\alpha)(\omega_k^2 - \sigma_k) - p_k s_k \omega_k^2}{s_k^2\omega_k^2 + q_k(\alpha)^2}, \end{aligned} \tag{25}$$

which implies that

$$\omega_k^4 + (p_k^2 - s_k^2 - 2\sigma_k)\omega_k^2 + \sigma_k^2 - q_k(\alpha)^2 = 0. \tag{26}$$

Denote

$$\omega_k^{\pm} := \sqrt{\frac{s_k^2 - p_k^2 + 2\sigma_k \pm \sqrt{(s_k^2 - p_k^2 + 2\sigma_k)^2 - 4(\sigma_k^2 - q_k(\alpha)^2)}}{2}}. \tag{27}$$

So, we first discuss the sign of $\sigma_k^2 - q_k(\alpha)^2 = (\sigma_k + q_k(\alpha))(\sigma_k - q_k(\alpha))$. Since $\sigma_k + q_k(\alpha) > 0$ is guaranteed by Theorem 7, the sign of $\sigma_k^2 - q_k(\alpha)^2$ coincides with that of $\sigma_k - q_k(\alpha)$, and

$$\sigma_k - q_k(\alpha) = (d_u k^2 + (a\bar{u} - \varpi))(d_v k^2 - c b_2 \varpi) - c b_2 \varpi^2 - k^2 c b_2 \bar{v}\varpi\alpha. \tag{28}$$

Because $\sigma_k - q_k(\alpha) = 0$ with respect to k has only one positive root, denoted as K^0 for simplicity, where

$$K^0 = \sqrt{\frac{-\Gamma + \sqrt{\Gamma^2 + 4 d_u d_v a c b_2 \bar{u}\varpi}}{2 d_u d_v}} \tag{29}$$

with $\Gamma := d_v(a\bar{u} - \varpi) - d_u c b_2 \varpi - \alpha c b_2 \bar{v}\varpi$, we can conclude that

$$\begin{aligned} \sigma_k^2 - q_k^2(\alpha) &< 0, \quad k \in (0, K^0), \\ \sigma_k^2 - q_k(\alpha)^2 &> 0, \quad k \in (K^0, \infty). \end{aligned}$$

And, the following theorem deals with the case about the roots of (26).

Theorem 8. For $a, b_1, b_2, m_1, d_v > 0$, provided that $c > \frac{m_1}{b_1}$, $r_0 > \underline{r_0}$, then for $d_u, \alpha > 0$ and $k \in \mathbb{N}_0$, it follows that

(1) when $0 \leqslant k < K^0$, ω_k^+ is the unique positive root of (26).

(2) when $k \geqslant K^0$, (26) has no positive root.

Proof. For $0 \leqslant k < K^0$, since $\sigma_k^2 - q_k^2(\alpha) < 0$, ω_k^+ is the only positive root of (26), regardless of the positivity or negativity of $s_k^2 - p_k^2 + 2\sigma_k$.

For $k \geqslant K^0$, the $\sigma_k^2 - q_k^2(\alpha) \geqslant 0$ holds, and it follows (28) that for $k = K^0$,

$$(d_u(K^0)^2 + (a\bar{u} - \varpi))(d_v(K^0)^2 - c b_2 \varpi) = c b_2 \varpi^2 + (K^0)^2 c b_2 \bar{v}\varpi\alpha > 0. \tag{30}$$

Note that

$$s_k^2 - p_k^2 + 2\sigma_k = -\left[(d_u k^2 + (a\bar{u} - \varpi))^2 + (d_v k^2 + c b_2 \varpi)(d_v k^2 - c b_2 \varpi)\right], \tag{31}$$

thus,

(a) if $\underline{r_0} < r_0 < \bar{r}_0$, that is to say, $a\bar{u} - \varpi < 0$, one can show that $s_k^2 - p_k^2 + 2\sigma_k = 0$ with respect to k has a unique positive root, denoted as K^+. And by (29), we have

$$2 d_u d_v (K^0)^2 = -\Gamma + \sqrt{\Gamma^2 + 4 d_u d_v a c b_2 \bar{u}\varpi}, \tag{32}$$

so it can be verified that

$$\begin{aligned} d_u(K^0)^2 + (a\bar{u} - \varpi) &= 2d_v(d_u(K^0)^2 + (a\bar{u} - \varpi)) \\ &= -\Gamma + \sqrt{\Gamma^2 + 4d_u d_v acb_2\bar{u}\varpi} + 2d_v(a\bar{u} - \varpi) \\ &> 2cb_2\varpi(d_u + \alpha\bar{v}) > 0, \\ d_v(K^0)^2 - cb_2\varpi &= 2d_u(d_v(K^0)^2 - cb_2\varpi) \\ &= -\Gamma + \sqrt{\Gamma^2 + 4d_u d_v acb_2\bar{u}\varpi} - 2d_u cb_2\varpi \\ &= -2d_v(a\bar{u} - \varpi) + 2\alpha cb_2\bar{v}\varpi > 0, \end{aligned} \tag{33}$$

which yields that $s_{K^0}^2 - p_{K^0}^2 + 2\sigma_{K^0} < 0$, that is to say, $s_k^2 - p_k^2 + 2\sigma_k < 0$ for $k \geqslant K^0 > K^+$. Hence, from (27), we know that (26) has no positive root for $k \geqslant K^0$.

(*b*) if $r_0 \geqslant \bar{r}_0$, that is to say, $a\bar{u} - \varpi \geqslant 0$, then $d_u(K^0)^2 + (a\bar{u} - \varpi) > 0$. It follows from (30) that $d_v(K^0)^2 - cb_2\varpi > 0$. By a similar argument to (*a*), (26) has no positive root for $k \geqslant K^0$, either.

□

Thus, due to Theorem 8, if the positive root $\omega_k = \omega_k^+$ of (26) exists, denote the root of (25) in $(0, 2\pi]$ as $\tau_k(\alpha)$. For $a, b_1, b_2, m_1, d_v > 0$, provided that $c > \frac{m_1}{b_1}$, $r_0 > \underline{r_0}$, then for $d_u, \alpha > 0$, denote the critical values for τ by

$$\tau_k^{(j)}(\alpha) := \tau_k(\alpha) + \frac{2\pi j}{\omega_k^+},\ j, k \in \mathbb{N}_0,\ 0 \leqslant k < K^0. \tag{34}$$

Suppose that $\lambda_2(k, \tau, \alpha) = \xi(k, \tau, \alpha) \pm \mathrm{i}\omega(k, \tau, \alpha)$ is a pair of conjugated complex roots of characteristic equation $D_k(\lambda, \tau, \alpha) = 0$ near $\tau = \tau_k^{(j)}(\alpha)$ with $\xi(k, \tau_k^{(j)}(\alpha), \alpha) = 0$, $\omega(k, \tau_k^{(j)}(\alpha), \alpha) = \omega_k^+ > 0$. According to[4,43], we obtain the conclusion regarding the transversality conditions.

Theorem 9. For $a, b_1, b_2, m_1, d_v > 0$, provided that $c > \frac{m_1}{b_1}$, $r_0 > \underline{r_0}$, then for $d_u, \alpha > 0$,

$$sign\left(\frac{d\xi(k, \tau_k^{(j)}(\alpha), \alpha)}{d\tau}\right) > 0,\ 0 \leqslant k < K^0,\ k \in \mathbb{N}_0.$$

Proof. For $0 \leqslant k < K^0$ and $k \in \mathbb{N}_0$, denote

$$P(\lambda) := \lambda^2 + p_k\lambda + \sigma_k,\ Q(\lambda) := s_k\lambda + q_k(\alpha).$$

Obviously, $P(\mathrm{i}\omega_k^+) + Q(\mathrm{i}\omega_k^+) \neq 0$. For $\forall\omega_k > 0$, define

$$F(\omega_k) := \mid P(\mathrm{i}\omega_k) \mid^2 - \mid Q(\mathrm{i}\omega_k) \mid^2 = (\sigma_k - \omega_k^2)^2 + \omega_k^2 p_k^2 - (\omega_k^2 s_k^2 + q_k(\alpha)^2). \tag{35}$$

Hence, $F(\omega_k) = 0$ implies that (26) holds, and its roots are given by (27). If denoting

$$\Delta_\omega := (s_k^2 - p_k^2 + 2\sigma_k)^2 - 4(\sigma_k^2 - q_k(\alpha)^2),$$

then for $\omega_k = \omega_k^+$, it follows that

$$2(\omega_k^+)^2 - (s_k^2 + 2\sigma_k - p_k^2) = \sqrt{\Delta_\omega} > 0. \tag{36}$$

By (35) and (36), we have

$$\frac{dF(\omega_k^+)}{d\omega_k} = 2\omega_k^+[2(\omega_k^+)^2 - (s_k^2 + 2\sigma_k - p_k^2)] = 2\omega_k^+\sqrt{\Delta_\omega} > 0. \tag{37}$$

By (25), define

$$S_k^{(j)}(\tau) := \tau - \frac{\theta_k(\alpha) + 2\pi j}{\omega_k^+},\ j \in \mathbb{N}_0,$$

with

$$\theta_k(\alpha) := \arccos\left(\frac{q_k(\alpha)((\omega_k^+)^2 - \sigma_k) - p_k s_k(\omega_k^+)^2}{s_k^2(\omega_k^+)^2 + q_k(\alpha)^2}\right).$$

It follows from (34) that

$$\tau_k^{(j)}(\alpha) := \tau_k(\alpha) + \frac{2\pi j}{\omega_k^+} = \frac{\theta_k(\alpha) + 2\pi j}{\omega_k^+},\ j \in \mathbb{N}_0$$

which is independent of τ. Therefore,

$$\frac{dS_k^{(j)}(\tau_k^{(j)}(\alpha))}{d\tau} = 1,\ j \in \mathbb{N}_0. \tag{38}$$

Then, by[4], we have

$$sign\left\{\frac{d\xi(k,\tau_k^{(j)}(\alpha),\alpha)}{d\tau}\right\} = sign\left\{\frac{dF(\omega_k^+)}{\omega_k}\right\} sign\left\{\frac{dS_k^{(j)}(\tau_k^{(j)}(\alpha))}{d\tau}\right\} > 0.$$

Thus, we complete the proof. □

Finally, we have the conclusion on the Hopf bifurcation of system (2).

Theorem 10. For $a, b_1, b_2, m_1, d_v > 0$, provided that $c > \frac{m_1}{b_1}$, $r_0 > \underline{r_0}$, then for $d_u, \alpha > 0$, there exists $k_2 \in [0, K^0)$ such that

$$\tau_{k_2}(\alpha) := \min_{k\in[0,K^0),\ k\in\mathbb{N}_0} \tau_k(\alpha). \tag{39}$$

So,

(1) when $\tau = \tau_{k_2}(\alpha)$, $D_{k_2}(\lambda, \tau, \alpha) = 0$ has a pair of purely imaginary roots for λ, and all other roots of (6) have strictly negative real parts for $k \in \mathbb{N}_0$. When $\tau \in \left[0, \tau_{k_2}(\alpha)\right)$, steady state $\bar{E}$ is locally asymptotically stable.

(2) if k_2 is unique, system (2) undergoes mode-k_2 Hopf bifurcation when $\tau = \tau_{k_2}(\alpha)$; and if there are exactly k_2 and $\tilde{k}_2$ satisfying (39), with $k_2, \tilde{k}_2 \in [0, K^0)$ and $k_2 \neq \tilde{k}_2$, system (2) will undergo mode-$(k_2, \tilde{k}_2)$ Hopf-Hopf bifurcation when $(\tau, \alpha) = (\tau_{k_2}(\alpha_H), \alpha_H)$, where α_H denotes the root of $\tau_{k_2}(\alpha) = \tau_{\tilde{k}_2}(\alpha)$.

Remark 2. **(Hopf patterns and Hopf-Hopf patterns)** In Theorem 8, the range of wave numbers in which system (2) undergoes Hopf bifurcation is completely determined, which is upper bounded by K^0.

Hopf bifurcation sets are given in Figure 7 (*a*), where some Hopf bifurcation curves for different modes are plotted, and the regions where multiple periodic patterns exist are marked, including Hopf bifurcation regions D_0^H, D_1^H, D_2^H where stable spatially homogeneous or inhomogeneous periodic patterns are expected to appear, Hopf-Hopf bifurcation regions $D_{0,1}^H$, $D_{1,2}^H$, $D_{2,3}^H$ where periodic patterns with different spatial wave frequencies coexist, or quasi-periodic patterns are anticipated to emerge.

And the corresponding first Hopf bifurcation curve is plotted in Figure 7 (*b*), which is formed by connecting Hopf bifurcation curves of mode-0, mode-1, mode-2, ⋯, mode-$\lfloor K^0 \rfloor$ with Hopf-Hopf bifurcation points $H_{0,1}, H_{1,2}, \ldots, H_{\lfloor K^0\rfloor-1,\lfloor K^0\rfloor}$, indicating that the positive constant steady state can be destabilized by mode-k Hopf bifurcation, thus system (2) will harvest the spatial homogeneous or inhomogeneous staggered periodic solutions shaped like $\cos kx \cos \omega t$, and also suggesting that the positive constant steady state can be destabilized by mode-$(k, k+1)$ Hopf-Hopf bifurcation, thus system (2) will harvest more complex spatiotemporal patterns, such as coexistence of periodic solutions with two different spatial wave frequencies, or some quasi-periodic solutions, where ω is a positive constant, and $0 \leqslant k < K^0, k \in \mathbb{N}_0$. This is completely different from systems with only self-diffusion[17,31], where the positive constant steady state can only be destabilized by mode-0 Hopf bifurcation, producing a stable spatially homogeneous periodic solution.

Combing Theorems 6 and 10, it is found that predator-taxis α and delay τ can induce other high co-dimensional bifurcations under certain conditions, such as Turing-Hopf bifurcation, etc.

Theorem 11. For $a, b_1, b_2, m_1, d_v > 0$, provided that $c > \frac{m_1}{b_1}$, $\underline{r_0} < r_0 < \bar{r}_0$, then

(1) if $d_u \in (d_u^{k_1,k_1+1}, d_u^{k_1-1,k_1})$ for some $k_1 \geqslant \bar{k}$ and $k_1 \in \mathbb{N}$, system (2) undergoes mode-(k_1, k_2) Turing-Hopf bifurcation near $\bar{E}$ when $(\tau, \alpha) = (\tau_{k_2}(\alpha_*(d_u)), \alpha_*(d_u))$, where $\bar{k}$ is defined as in (14) and k_2 is uniquely determined by (39).

(2) if $d_u \in (d_u^{k_1,k_1+1}, d_u^{k_1-1,k_1})$ for some $k_1 \geqslant \bar{k}$ and $k_1 \in \mathbb{N}$, system (2) will undergo mode-$(k_1, k_2, \tilde{k}_2)$ Turing-Hopf-Hopf bifurcation near $\bar{E}$ when $(d_u, \tau, \alpha) = (d_u^H, \tau_{k_2}(\alpha_H), \alpha_H)$, where d_u^H denotes the root of $\alpha_*(d_u) = \alpha_H$, and α_H is defined in Theorem 10, $\bar{k}$ is defined as in (14) and $k_2, \tilde{k}_2$ are determined by Theorem 10.

(3) if $d_u = d_u^{k_1,k_1+1}$ for some $k_1 \geqslant \bar{k}$ and $k_1 \in \mathbb{N}$, system (2) will undergo mode-(k_1, k_1+1, k_2) Turing-Turing-Hopf bifurcation near $\bar{E}$ when $(d_u, \tau, \alpha) = (d_u^{k_1,k_1+1}, tau_{k_2}(\alpha_*(d_u^{k_1,k_1+1})), \alpha_*(d_u^{k_1,k_1+1}))$, where $\bar{k}$ is defined as in (14) and k_2 is determined by (39).

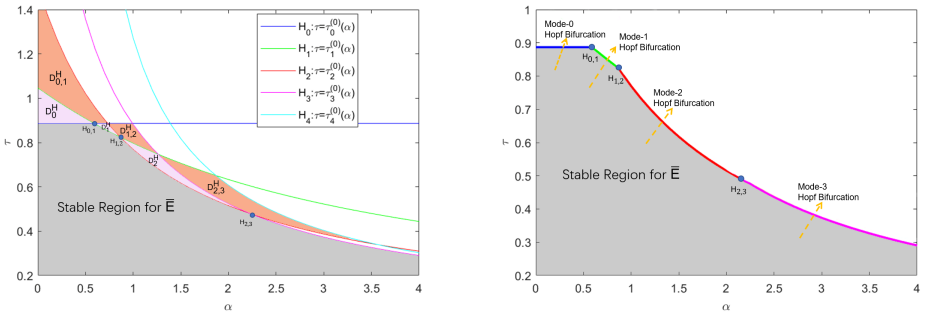

(a) (b)

Figure 7 (*a*): Stable region, Hopf bifurcation regions and Hopf-Hopf bifurcation regions. (*b*): The first Hopf bifurcation curve. The non-smooth points $H_{0,1}$, $H_{1,2}$, $\cdots$ are Hopf-Hopf bifurcation points.

Next, we illustrate some examples to support and extend our analytical results.

With reference to parameter selections in [37], let

$$\begin{aligned} r_0 =&2.1155,\ a = 0.8481,\ b_1 = 4.5677,\\ m_1 =&1.6615,\ c = 0.9130,\ b_2 = 1.4380. \end{aligned} \tag{40}$$

Then (9) is satisfied, and $\bar{E} = (0.2412, 0.2533)$ is locally asymptotically stable for local ODE system.

In the following discussions, we observe that the spatiotemporal distribution types of the two populations are always analogous. Therefore, we only take the prey distribution as examples to show distribution patterns. Besides, the distribution patterns in (u, x, t)-plane and (x, t)-plane are presented separately in each of the following figures.

Example 3. (Hopf bifurcation and spatially inhomogeneous staggered periodic patterns, Hopf-Hopf bifurcation and bistable periodic patterns)

Let

$$d_v = 0.17,\ d_u = 0.113.$$

It follows (14) that $\bar{k} = 3$ and $d_u > d_u^{\bar{k}} = 0.0284$, then due to Theorem 6, for $\alpha > 0$, positive steady state $\bar{E}$ is locally asymptotically stable. According to Theorem 10, Hopf bifurcation curves in (α, τ)-plane for different modes can be characterized as in Figure 7. And

$$\begin{aligned} &\alpha_H^{0,1} = 0.5846,\ \alpha_H^{0,2} = 0.7487,\ \alpha_H^{1,2} = 0.8554,\\ &\alpha_H^{1,3} = 1.2704,\ \alpha_H^{2,3} = 2.2277. \end{aligned}$$

When

$$\alpha \in (0, \alpha_H^{0,1}),\ \alpha \in (\alpha_H^{0,1}, \alpha_H^{1,2}),\ \alpha \in (\alpha_H^{1,2}, \alpha_H^{2,3}),$$

respectively, either $\bar{E}$ is locally asymptotically stable or system (2) may accordingly generate stable spatially homogeneous periodic patterns, spatially inhomogeneous periodic patterns with spatial wave frequency 1 or 2, which are bifurcated from $\bar{E}$ through mode-0, mode-1 and mode-2 Hopf bifurcation respectively.

Further, when

$$\alpha \in (\alpha_H^{0,1}, \alpha_H^{0,2}),\ \alpha \in (\alpha_H^{0,2}, \alpha_H^{1,3}),$$

respectively, in addition to the above mentioned periodic patterns, system (2) may also generate quasi-periodic patterns, the coexisting periodic patterns with different spatial wave frequencies, which are bifurcated from $\bar{E}$ through mode-$(0, 1)$ and mode-$(1, 2)$ Hopf-Hopf bifurcation, respectively. Specifically speaking,

(1) Let $(\alpha, \tau) = (1.2, 0.72)$. By (32), we have $K^0 = 5.1978$, and

$$\begin{aligned} &\tau_0^{(0)}(1.2) = 0.8870,\ \tau_1^{(0)}(1.2) = 0.7585,\\ &\tau_2^{(0)}(1.2) = 0.7004,\ \tau_3^{(0)}(1.2) = 0.7748,\\ &\tau_4^{(0)}(1.2) = 1.0375,\ \tau_5^{(0)}(1.2) = 2.8230. \end{aligned} \tag{41}$$

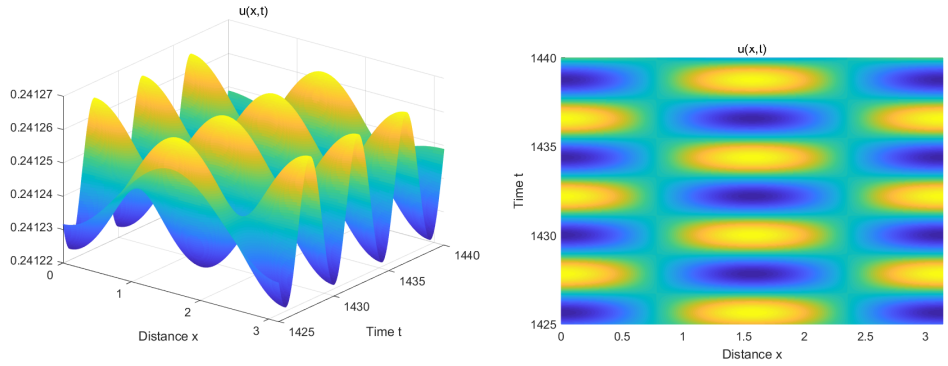

Figure 8 Let $(\alpha, \tau) = (1.2, 0.72)$, then spatially inhomogeneous staggered periodic patterns with wave frequency 2 appear.

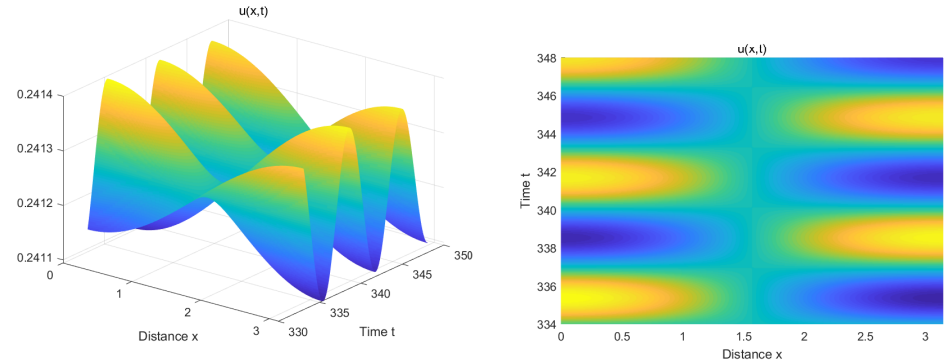

Figure 9 Let $(\alpha, \tau) = (0.7, 0.87)$, then spatially inhomogeneous staggered periodic patterns with wave frequency 1 appear.

Thus, $(\alpha, \tau) \in D_2^H$. It follows Theorem 10 that system (2) undergoes mode-2 Hopf bifurcation when $\tau = \tau_2^{(0)}(1.2) = 0.7004$ and spatially inhomogeneous staggered periodic patterns shaped like $\cos 2x \cos \omega t$ are theoretically expected to appear, where ω is a positive constant. The numerical results are shown in Figure 8.

Let $(\alpha, \tau) = (0.7, 0.87)$, then by a similar process, $(\alpha, \tau) \in D_1^H$, thus system (2) undergoes mode-1 Hopf bifurcation when $\tau = \tau_1^{(0)}(0.7) = 0.8607$, and spatially inhomogeneous staggered periodic patterns shaped like $\cos x \cos \omega t$ are theoretically expected to appear, where ω is a positive constant, see Figure 9.

(2) Let $(\alpha, \tau) = (0.61, 0.91364)$. By (32), we have $K^0 = 4.4040$, and

$$\begin{aligned} &\tau_0^{(0)}(0.61) = 0.8870, \ \tau_1^{(0)}(0.61) = 0.8819, \\ &\tau_2^{(0)}(0.61) = 0.9525, \ \tau_3^{(0)}(0.61) = 1.2115, \\ &\tau_4^{(0)}(0.61) = 2.4037. \end{aligned} \tag{42}$$

Thus $(\alpha, \tau) \in D_{0,1}^H$. Then bistable spatiotemporal periodic patterns shaped like $\cos \omega t$ and $\cos x \cos \omega t$ or their superposition are theoretically expected to appear, where ω is a positive constant. When choosing $(0.2412, 0.2533)$ and $(0.2412+0.01\cos x, 0.2533+0.01\cos x)$ as initial values respectively, as shown in the first two columns of Figure 10, spatially homogeneous and inhomogeneous staggered periodic patterns coexist. When choosing $(0.2412, 0.2533+0.01\cos x)$ as an initial value, transient quasi-periodic patterns are presented in the third column of Figure 10. Hence, these phenomena are bistable periodic patterns.

Let $(\alpha, \tau) = (0.87, 0.8415)$, then by a similar process, we know that $(\alpha, \tau) \in D_{1,2}^H$. Then spatiotemporal periodic patterns shaped like $\cos x \cos \omega t$ and $\cos 2x \cos \omega t$ or their superposition are theoretically expected to appear, where ω is a positive constant. When choosing $(0.2412 + 0.01\cos x, 0.2533 + 0.01\cos x)$ and $(0.2412 + 0.01\cos 2x, 0.2533 + 0.01\cos 2x)$ as

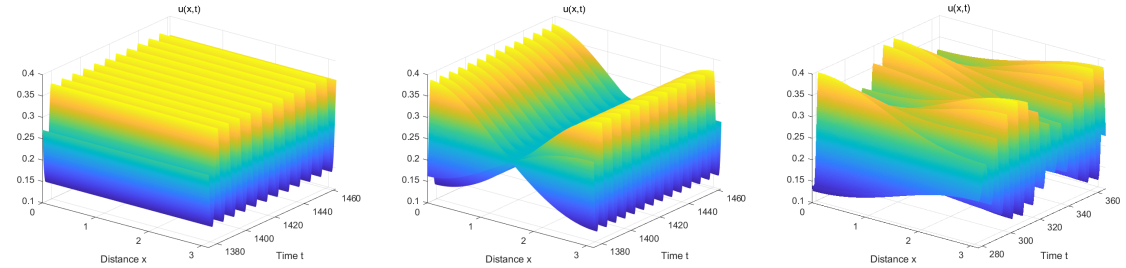

(a) Spatially homogeneous, inhomogeneous straggered periodic patterns and transient quasi-periodic patterns, respectively.

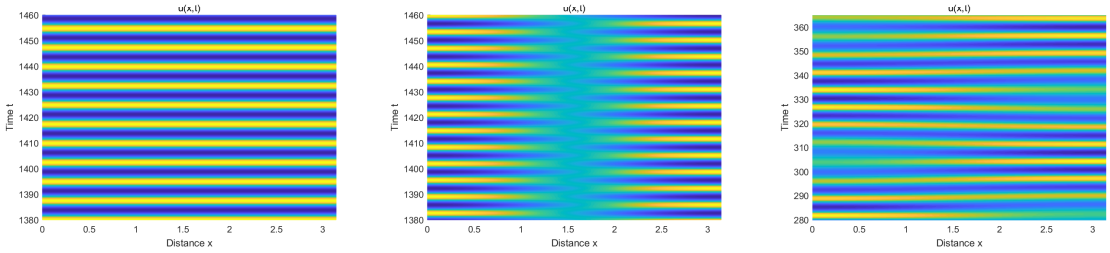

(b) The according projections of (a) on (x,t)-plane.

Figure 10 Bistable periodic patterns and transient quasi-periodic patterns when $(\alpha,\tau)=(0.61,0.91364)$.

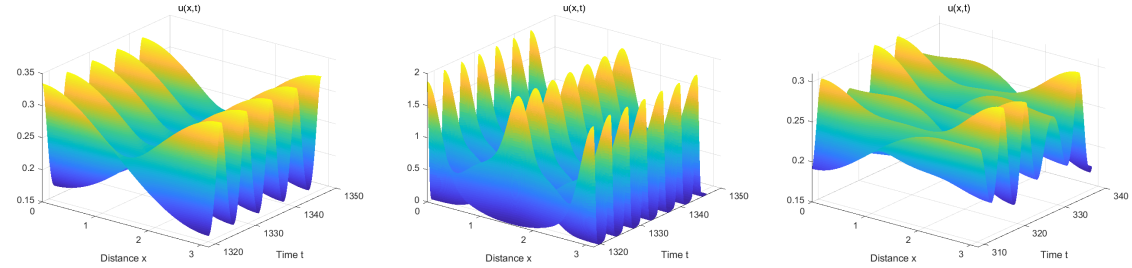

(a) Spatially inhomogeneous staggered periodic patterns with spatial wave frequencies 1, 2, and transient quasi-periodic patterns, respectively.

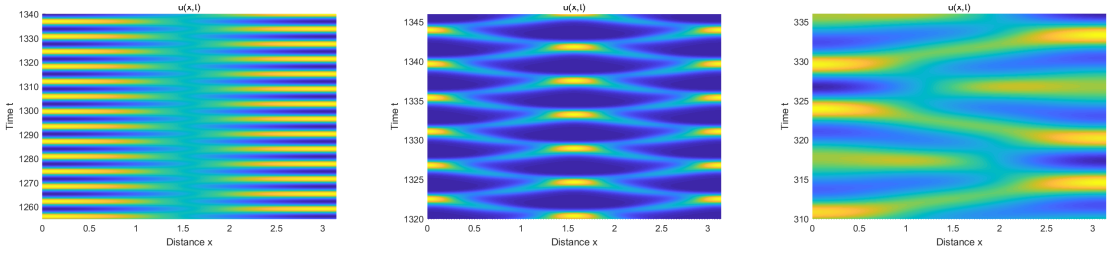

(b) The according projections of (a) on (x,t)-plane.

Figure 11 Bistable periodic patterns and transient quasi-periodic patterns when $(\alpha,\tau)=(0.87,0.8415)$.

initial values respectively, as shown in the first two columns of Figure 11, spatially inhomogeneous staggered periodic patterns with wave frequencies 1 and 2 coexist. When further choosing $(0.2412+0.01\cos x, 0.2533+0.01\cos 2x)$ as an initial value, transient quasi-periodic patterns are presented in the third column of Figure 11. That is, bistable periodic patterns are also found, but the spatial wave frequencies are different from those shown in Figure 10.

Example 4. (Turing-Hopf bifurcation and bistable spatially inhomogeneous synchronous periodic patterns)
Let

$$d_v=0.17,\ d_u=0.0113,$$

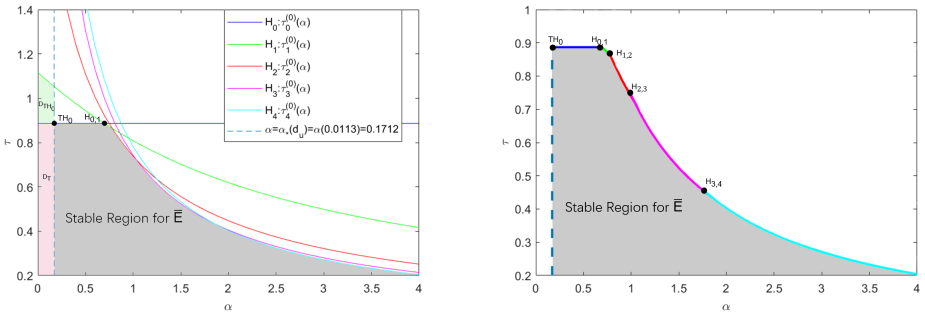

(a) (b)

Figure 12 (*a*): Turing-Hopf bifurcation sets in (α, τ)-plane. (*b*): The first bifurcation curve. The point TH_0 is a mode-$(3,0)$ Turing-Hopf bifurcation point. The points $H_{0,1}, H_{1,2}, \cdots$ are Hopf-Hopf bifurcation points.

then $d_u \in (d_u^{3,4}, d_u^{1,2}) = (0.0084, 0.0334)$, and by Theorems 6 and 10, we conclude $k_1 = 3, k_2 = 0$. It follows Theorem 11 that system (2) undergoes mode-$(3,0)$ Turing-Hopf bifurcation when $(\tau, \alpha) = (\tau_0(\alpha_*(0.113)), \alpha_*(0.113)) = (0.887, 0.1712)$.

We plot the according bifurcation sets for system (2) in Figure 12 (*a*), and the intersection of mode-3 Turing bifurcation curve $\alpha = \alpha_*(0.0113) = 0.1712$ and mode-0 Hopf bifurcation curve $\tau = \tau_* = 0.8870$ is denoted by TH_0. We mark Turing-Hopf bifurcation region and Turing bifurcation region as D_{TH_0} and D_T, respectively.

In particular, we plot the corresponding first bifurcation curve in Figure 12 (*b*), which is formed by connecting the first Turing bifurcation curve $\alpha = \alpha_*(d_u)$, $0 < d_u < d_u^{\bar{k}}$, Hopf bifurcation curves of mode-0, mode-1, mode-2, … , mode-$\lfloor K^0 \rfloor$ with Turing-Hopf bifurcation point TH_0, Hopf-Hopf bifurcation points $H_{0,1}$, $H_{1,2}$, … , $H_{\lfloor K^0 \rfloor - 1, \lfloor K^0 \rfloor}$, indicating that the positive constant steady state can be not only destabilized by mode-k_2 Hopf bifurcation or mode-(k_2, k_2+1) Hopf-Hopf bifurcation, but also by mode-$(k_1, 0)$ Turing-Hopf bifurcation, where system (2) will harvest the spatial inhomogeneous synchronous periodic solutions shaped like $h_1 \cos k_1 x \pm h_2 \cos \omega t$, where h_1, h_2 are constants, ω is a positive constant, $k_1 = \bar{k}, \bar{k}+1, \cdots$ and $0 \leqslant k_2 < K^0, k_2 \in \mathbb{N}_0$.

Further, let $(\alpha, \tau) = (0.06, 0.9) \in D_{TH_0}$, and we find a pair of stably coexisting spatially inhomogeneous synchronous periodic patterns, as shown in Figure 13. Differing from Figure 8 and Figure 9, the spatial non-homogeneity is caused by the occurrence of Turing bifurcation in system (2). Actually, Turing-Hopf bifurcation can also reveal other spatiotemporal patterns [15,16], which we will explore later.

Remark 3. **(Turing-Hopf patterns and other patterns)** Although it is almost impossible to theoretically prove that for system (2) with chemotaxis, Turing-Hopf bifurcation of mode-$(k,0)$ usually occurs first when the positive constant steady state is destabilized via Turing-Hopf bifurcation, some numerical simulations indicate that stable spatially inhomogeneous synchronous periodic solutions can only be generated through mode-$(k,0)$ Turing-Hopf bifurcation.

In Theorem 11, we assert that Turing-Turing-Hopf bifurcation can occur theoretically, but it is challenging to reveal spatiotemporal patterns resulting from this type of bifurcation. In addition, although we can not rule out the existence of Turing-Hopf-Hopf bifurcation theoretically, we never numerically find Turing-Turing-Hopf bifurcation points after massive numerical practices. But obviously, if Turing-Hopf bifurcation points, such as TH_1, $TH_2, \cdots$ do not exist, Turing-Turing-Hopf bifurcation must not occur.

Summarizing the results about Turing bifurcation in Section 3 and Hopf bifurcation in Section 4 in Table 2, we show the possible bifurcations for system (2) when the parameters are chosen in different ranges. For convenience, we use notations T-T, H-H, T-H, T-H-H and T-T-H instead of Turing-Turing, Hopf-Hopf, Turing-Hopf, Turing-Hopf-Hopf and Turing-Turing-Hopf bifurcations.

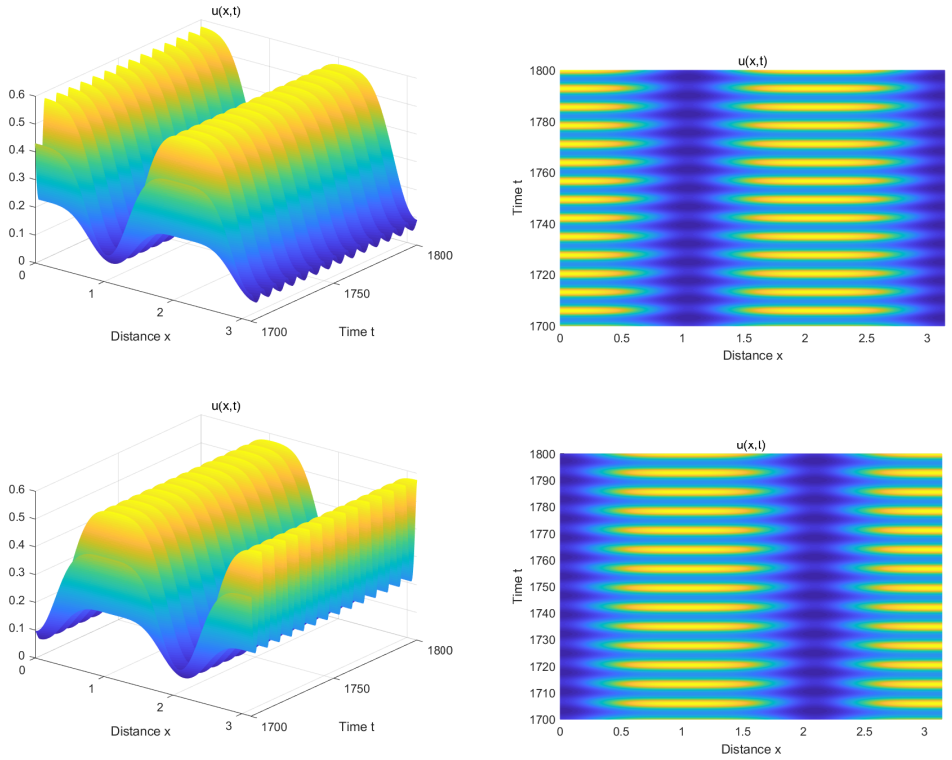

Figure 13 Let $(\alpha, \tau) = (0.06, 0.9)$, then a pair of spatially inhomogeneous synchronous periodic patterns coexist.

Table 2 The possible bifurcations for system (2).

r_0	d_u	α	τ	Turing	Hopf	Other	Theorems
$\geqslant r_0$	> 0	> 0	0	-	-	-	6, 7
			$\tau_{k_2}(\alpha)$	-	Yes	H-H	6, 10
$< r_0$	$\geqslant d_u^{\bar{k}}$	> 0	0	-	-	-	6, 7
			$\tau_{k_2}(\alpha)$	-	Yes	H-H	6, 10
$< r_0$	$< d_u^{\bar{k}}$	$\alpha_*(d_u)$	0	Yes	-	-	6, 7
			$\tau_{k_2}(\alpha)$	Yes	Yes	T-H, H-H or T-H-H	6, 10, 11
$< r_0$	$d_u^{k_1,k_1+1}$	$\alpha_*(d_u)$	0	Yes	-	T-T	6, 7
			$\tau_{k_2}(\alpha)$	Yes	Yes	T-T-H	6, 10, 11

5 | CONCLUSIONS

The formation mechanisms of populations' survival patterns in a predator-taxis model with conversion delay, such as multi-stable spatial patterns and spatially staggered periodic patterns, are discussed by studying Turing bifurcation, Turing-Turing bifurcation, Hopf bifurcation, Hopf-Hopf bifurcation, Turing-Hopf bifurcation of system (2), among others.

In the absence of a delayed effect of conversion of capture behavior into predator growth, the critical condition $0 < \alpha < \alpha_*(d_u)$, $0 < d_u < d_u^{\bar{k}}$ that positive constant steady state loses stability and system (2) exhibits spatial patterns is provided, which is not only sufficient but also necessary, thus can be regarded as a supplement to the sufficient conditions in [37]. With the aid of the condition, one can predict potential spatial patterns with arbitrary wave frequencies that system (2) could exhibit. In addition to this, it is also theoretically expected that positive constant steady state will be destabilized through Turing-Turing bifurcation, resulting in superposition spatial patterns or the co-existences of spatially inhomogeneous patterns with different

wave frequencies, see Theorem 6 and Figures 5, 6. Moreover, we suggest that the amplitude of changes in the spatial distributions of the two populations are consistent with the corresponding eigenfunctions when Turing bifurcation occurs.

The above results theoretically show that with the increase of the sensitivity of the prey to predation, the spatial distributions of the two populations will gradually transition from spatially heterogeneous patterns to spatially homogeneous patterns, see Figures 3-4. Conversely, when the random movement speed of prey is sufficiently small or the random movement speed of predator is sufficiently large, the spatial distributions homogeneity of the two populations disappear and heterogeneity appears, see Figures 3, 5 or Figures 3, 6. In other words, relatively large predator-taxis can be regarded as accelerating the self-diffusion of prey by complementing the self-diffusion of prey, and make two populations achieve their steady states eventually. And larger self-diffusion rate of predator is equivalent to lowering prey's ability to avoid the risk of predation, causing the spatial distributions of the two populations to be heterogeneous, whereas the relatively large predator-taxis counteracts the spatially heterogeneity distributed caused by the self-diffusion of predator, bringing the spatial distributions of the two populations back to homogeneity.

When taking a delayed effect of conversion of capture behavior into predator growth into account, by choosing time delay τ as a parameter, we establish the critical conditions when $\bar{E}$ is destabilized, which demonstrate that Hopf bifurcation, Hopf-Hopf bifurcation, Turing-Hopf bifurcation, etc., can also destabilize the positive constant steady state, see Theorems 10 and 11, leading to various spatiotemporal periodic patterns, such as stable spatially inhomogeneous staggered periodic patterns (Figures 8, 9), bistable spatiotemporal periodic patterns that two stable periodic patterns with different spatial wave frequencies coexist (Figures 10, 11), stable spatially inhomogeneous synchronous periodic pattern (see Figure 13) and so on.

These phenomena are different from the results for the ratio-dependent predator-prey system without predator-taxis in[31]. We assert that the existences of stable spatially inhomogeneous staggered periodic patterns and coexistence of bistable spatiotemporal periodic patterns are due to the addition of predator-taxis term. Therefore, the chemotactic behavior of prey makes the populations' survival patterns more diverse.

Further, there are still some issues to be resolved in theory. One is how to provide a definite order for these finite Hopf bifurcation curves when the system generates stable spatially inhomogeneous periodic solutions via mode-k ($0 \leqslant k < K^0$) Hopf bifurcation, as have been done for sorting Turing bifurcation curves in Lemma 4. Moreover, since we only numerically find that it is always mode-$(k, 0)$ Turing-Hopf bifurcation destabilizes the positive constant steady state, how to prove this finding theoretically is still a problem. Finally, it is worth mentioning that some other new spatiotemporal patterns can also arise via Turing-Turing bifurcation, Hopf-Hopf bifurcation, Turing-Hopf bifurcation, and Turing-Turing-Hopf bifurcation as expected by theory, so it will be of interest to establish the existences of other coexistence patterns analytically. We leave them as possible future work.

ACKNOWLEDGMENTS

The research is supported by the National Natural Science Foundation of China (No. 11871176).

Author contributions

This work was researched collaboratively by all authors, and the whole process was discussed for many times. The main manuscript text was finally written by Xing Yue and Cao Xun, and supervised by Jiang Weihua. All authors reviewed the manuscript.

Financial disclosure

None reported.

Conflict of interest

The authors declare no potential conflict of interests.

DATA AVAILABILITY STATEMENT

Data sharing not applicable to this article as no datasets were generated or analysed during the current study.

ETHICS APPROVAL STATEMENT

This declaration was not applicable because real human and/or animal researches were not involved in the current study.

References

1. H. Amann, Dynamic theory of quasilinear parabolic equations. II. Reaction-diffusion systems. Differential Integral Equations 3(1) (1990) 13-75.

2. I. Ahn, C. Yoon, Global well-posedness and stability analysis of prey-predator model with indirect prey-taxis. J Differential Equations 268(8) (2020) 4222-4255.

3. E. Beretta, Y. Kuang, Convergence results in a well-known delayed predator-prey system. J. Math. Anal. Appl. 204(3) (1996) 840-853.

4. E. Beretta, Y. Kuang, Geometric stability switch criteria in delay differential systems with delay dependent parameters. SIAM J. Math. Anal. 33(5) (2002) 1144-1165.

5. Q. Cao, J. Wu, Pattern formation of reaction-diffusion system with chemotaxis terms. Chaos 31(11) (2021) 113118.

6. X. Cao, X. Chen, W. Jiang, Bogdanov-Takens bifurcation with Z_2 symmetry and spatiotemporal dynamics in diffusive Rosenzweig-MacArthur model involving nonlocal prey competition. Discrete Contin. Dyn. Syst. 42 (2022) 3747-3785.

7. S. Chen, J. Yu, Stability analysis of a reactiondiffusion equation with spatiotemporal delay and Dirichlet boundary condition. J. Dynam. Differential Equations 28 (2016), 857-866.

8. S. Guo, Bifurcation and spatio-temporal patterns in a diffusive predator-prey system. Nonlinear Anal. Real World Appl. 42 (2018) 448-477.

9. J. Gao, S. Guo, Effect of prey-taxis and diffusion on positive steady states for a predator-prey system. Math. Methods. Appl. Sci. 41(10) (2018) 3570-3587.

10. X. Guo, J. Wang, Dynamics and pattern formations in diffusive predator-prey models with two prey-taxis. Math. Methods Appl. Sci. 42(12) (2019) 4197-4212.

11. D. Geng, W. Jiang, Y. Lou, H. Wang, Spatiotemporal patterns in a diffusive predator-prey system with nonlocal intraspecific prey competition. Stud. Appl. Math. 148(1) (2021) 396-432

12. X. Gao, Global solution and spatial patterns for a ratio-dependent predator-prey model with predator-taxis. Results Math. 77(2) (2022) 66

13. J. Huang, S. Ruan, J. Song, Bifurcations in a predator-prey system of Leslie type with generalized Holling type III functional response. J. Differential Equations 257(6) (2014) 1721-1752.

14. H. Jin, Z. Wang, Global stability of prey-taxis systems. J. Differential Equations 262(3) (2017) 1257-1290.

15. W. Jiang, H. Wang, X.Cao, Turing instability and Turing-Hopf bifurcation in diffusive Schnakenberg systems with gene expression time delay. J. Dynam. Differential Equations 31(4) (2019) 2223-2247.

16. W. Jiang, Q. An, J. Shi, Formulation of the normal form of Turing-Hopf bifurcation in partial functional differential equations. J. Differential Equations 268(10) (2020) 6067-6102.

17. X. Jiang, R. Zhang, Z. She, Dynamics of a diffusive predatorprey system with ratio-dependent functional response and time delay. Int. J. Biomath. 13(6) (2020) 2050036.

18. Y. Kuang, Delay differential equations with applications in population dynamics. Academic Press, New York (1993)

19. M. Kuwamura, Turing instabilities in preypredator systems with dormancy of predators. J. Math. Biol. 71 (2015) 125-149.

20. J. M. Lee, T. Hillen, M. A.Lewis, Pattern formation in prey-taxis systems. J. Biol. Dyn. 3(6) (2009) 551-573.

21. Z. Ling, L. Zhang, Z. Lin, Turing pattern formation in a predatorprey system with cross diffusion. Appl. Math. Model. 38(21) (2014) 5022-5032.

22. Y. Liu, J. Wei, Dynamical analysis in a diffusive predator-prey system with a delay and strong Allee effect. Math. Methods Appl. Sci. 43(4) (2020) 1590-1607.

23. Y. Lou, H. Nie, Global dynamics of a generalist predatorprey model in open advective environments. J. Math. Biol. 84(6) (2022) 1-40.

24. C. Liu, S. Guo, Dynamics of a predatorprey system with nonlinear prey-taxis. Nonlinearity 35 (2022) 4283.

25. P. Mishra, D. Wrzosek, The role of indirect prey-taxis and interference among predators in pattern formation. Math. Methods Appl. Sci. 43(18) (2020) 10441-10461.

26. S. Mishra, R. Upadhyay, Kumar Spatial pattern formation and delay induced destabilization in predator-prey model with fear effect. Math. Methods Appl. Sci. 45(11) (2022) 6801-6823.

27. H. Qiu, S. Guo, S. Li, Stability and bifurcation in a predatorprey system with prey-taxis. Internat. J. Bifur. Chaos Appl. Sci. Engrg. 30(02) (2020) 2050022.

28. S. Ruan, On nonlinear dynamics of predator-prey models with discrete delay. Math. Model. Nat. Phenom. 4(2) (2009) 140-188.

29. J. Shi, C. Wang, H. Wang, Spatial movement with diffusion and memory-based self-diffusion and cross-diffusion. J. Differential Equations 305 (2021) 242-269.

30. Y. Song, X. Zou, Bifurcation analysis of a diffusive ratio-dependent predatorprey model. Nonlinear Dyn. 78(1) (2014) 49-70.

31. Y. Song, Y. Peng, X. Zou, Persistence, stability and Hopf bifurcation in a diffusive ratio-dependent predator-prey model with delay. Internat. J. Bifur. Chaos Appl. Sci. Engrg. 24(7) (2014) 995-49.

32. N. Tania, B. Vanderlei, J. P.Heath, L. Edelstein-Keshet, Role of social interactions in dynamic patterns of resource patches and forager aggregation. Proc. Natl. Acad. Sci. USA 109(28) (2012) 11228-11233.

33. M. Winkler, Boundedness in the higher-dimensional parabolic-parabolic chemotaxis system with logistic source. Comm. Partial Differential Equations 35(8) (2010) 1516-1537.

34. S. Wu, J. Shi, B. Wu, Global existence of solutions and uniform persistence of a diffusive predator-prey model with prey-taxis. J. Differential Equations 260(7) (2016) 5847-5874.

35. S. Wu, J. Wang, J. Shi, Dynamics and pattern formation of a diffusive predator-prey model with predator-taxis. Math. Models Methods Appl. Sci. 28(11) (2018) 1-36.

36. X. Wang, W. Wang, G. Zhang, Global bifurcation of solutions for a predator-prey model with prey-taxis. Math. Methods Appl. Sci. 38(3) (2015) 431-443.

37. X. Wang, X. Zou, Pattern formation of a predator-prey model with the cost of anti-predator behaviors. Math. Biosci. Eng. 15(3) (2018) 775-805.

38. J. Wang, S. Wu, J. Shi, Pattern formation in diffusive predator-prey systems with predator-taxis and prey-taxis. Discrete Contin. Dyn. Syst. Ser. B. 26(3) (2021) 1273.

39. M. Wang, Second Order Nonlinear Parabolic Equations. CRC Press (2021)

40. C. Wang, S. Yuan, H.Wang, Spatiotemporal patterns of a diffusive prey-predator model with spatial memory and pregnancy period in an intimidatory environment. J. Math. Biol. 84(3) (2022) 1-36.

41. J. Xia, Z. Liu, R. Yuan, S. Ruan, The effects of harvesting and time delay on predator-prey systems with Holling type II functional response. SIAM J. Appl. Math. 70(4) (2009) 1178-1200.

42. T. Xiang, Global dynamics for a diffusive predator-prey model with prey-taxis and classical Lotka-Volterra kinetics. Nonlinear Anal. Real World Appl. 39 (2018) 278-299.

43. F. Yi, E. A. Gaffney, S. Seirin Lee, The bifurcation analysis of Turing pattern formation induced by delay and diffusion in the Schnakenberg system. Discrete Contin. Dyn. Syst. Ser. B. 22(2) (2017) 647-668.

44. R. Yang, F. Wang, D. Jin, Spatially inhomogeneous bifurcating periodic solutions induced by nonlocal competition in a predator-prey system with additional food. Math. Methods Appl. Sci. 45(16) (2022) 9967-9978.

How to cite this article: Yue Xing, Weihua Jiang, Xun Cao (2023), Multi-stable and spatiotemporal staggered patterns in a predator-prey model with predator-taxis and delay, *Math. Methods Appl. Sci.*, *2023;00:1–24*.